Journal of Atmospheric and Solar–Terrestrial Physics 209 (2020) 105398

Contents lists available at ScienceDirect

Journal of Atmospheric and Solar-Terrestrial Physics

journal homepage: www.elsevier.com/locate/jastp

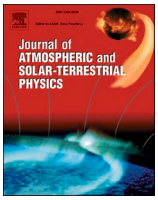

Impact of solar irradiance and geomagnetic activity on polar NOx, ozone and temperature in WACCM simulations

N. Tartaglione [a,b,*], T. Toniazzo [a,b], Y. Orsolini [b,c,d], O.H. Otterå [a,b]

[a] NORCE Norwegian Research Centre, Bergen, Norway
[b] Bjerknes Centre for Climate Research, Bergen, Norway
[c] Birkeland Centre for Space Science, University of Bergen, Bergen, Norway
[d] Norwegian Institute for Air Research, Kjeller, Norway

ARTICLE INFO

Keywords:
Stratosphere
Climate
Solar irradiance
Geomagnetic activity

ABSTRACT

The response of the atmosphere to solar irradiance and geomagnetic activity is analyzed in experiments with the Whole Atmosphere Community Climate Model (WACCM) under idealized forcings. Four experiments are carried out combining high (H) and low (L) solar radiative forcing with high (7) and low (3) geomagnetic activity: H7 (with high radiative forcing and high geomagnetic activity), H3, (high/low), L7 (low/high), and L3 (low/low). The comparison between these experiment is used to assess the effects of solar radiative forcing and geomagnetic activity mainly on the stratosphere. A two-step Monte Carlo-based statistical test, which defines an impact score, is used to assess statistically significant impacts on regional scales, on pressure levels, for a few key model variables, like NOx, ozone, and temperature.

Under low solar forcing (L7/L3), a statistically significant relationship between geomagnetic activity and NOx is found in both hemispheres and for all seasons. An equally strong relationship is lacking for ozone and temperature when analyzing these fields on isobaric levels. A statistically significant impact on stratospheric ozone is only seen in austral winter and spring. However, vertical cross sections show statistically significant impact on temperature and ozone mainly in the southern hemisphere (SH) during austral winter and the following spring.

Significant and persistent signals in both SH NOx and ozone concentrations are only produced when the effect of high solar forcing is added to high geomagnetic activity (H7). In this case, statistically significant differences are also found for mesospheric temperatures, ozone and NOx. This latter result appears also under low geomagnetic activity as a result of solar forcing alone, suggesting that solar irradiance significantly affects NOx, ozone and stratospheric temperatures and, in some seasons, even tropospheric temperature.

In summary, geomagnetic activity primarily affects NOx and ozone concentrations in the SH. Solar maximum conditions can reduce the amount of NOx in the stratosphere because of higher ozone production. Thus, we conclude that correlations between changes in solar irradiance and geomagnetic activity are important with respect to their effects on the atmosphere. In particular, geomagnetic activity can modulate atmospheric ozone concentrations and other associated stratospheric and tropospheric variables under conditions of high solar activity.

1. Introduction

The Earth's atmosphere is subject to both continuous energetic electron precipitation (EEP) and more intense precipitation events associated with solar activity, like solar proton events. Solar proton events occur mainly during solar maximum conditions and have a substantial effect on the chemical composition of the upper atmosphere (Heath et al., 1977; Jackman and McPeters, 2004). EEP encompasses medium- and high-energy electrons and auroral electrons. EEP events are less energetic but more frequent than solar proton events. Their injection into the atmosphere is steered by geomagnetic activity (GA), which is driven by high-speed solar wind streams and coronal mass ejections (Myllys et al., 2015). In the present observational period, GA follows a rough cycle, somewhat delayed in phase with respect to the 11-year solar cycle (Fraser-Smith, 1972; Echer et al., 2004; Du, 2011).

The main mechanism by which EEP influences the atmosphere is its

* Corresponding author. NORCE Norwegian Research Centre, Bergen, Norway.
E-mail address: nazario.tartaglione@norceresearch.no (N. Tartaglione).

https://doi.org/10.1016/j.jastp.2020.105398
Received 26 February 2020; Received in revised form 17 July 2020; Accepted 19 July 2020
Available online 29 July 2020

impact on the chemistry of nitrogen oxides (NOx) and hydrogen oxides that tend to deplete ozone catalytically. Auroral precipitation produces NOx in the lower thermosphere, while more episodic EEP events can produce NOx in the lower mesosphere (Garcia, 1992). The NOx can then be transported downward into the stratosphere at high latitudes in the winter season (Funke et al., 2005; Garcia, 1992; Solomon et al., 1999). Confined in darkness by the polar vortex (e.g. Solomon et al., 1982), NOx is long-lived, especially in the SH where the vortex is more stable, and contributes to catalytically reducing the amount of ozone as sunlight returns (Baumgaertner et al., 2009; Callis et al., 1996, 2001; Funke et al., 2005; Orsolini et al., 2005, 2017; Randall et al., 1998, 2001; 2005; Seppälä et al., 2007).

Ozone in the stratosphere has an important role in the radiative budget, as it absorbs short-wave radiation in the range of 200–400 nm. The absorption of ultraviolet (UV) radiation causes ozone photolysis and produces local warming of the mid-lower stratosphere. Ozone also absorbs long-wave radiation in the band centered at 1043 cm^{-1} (9.6 μm), which contributes to cooling the middle and upper stratosphere and warming the lower stratosphere (Baumgaertner et al., 2011; Brasseur and Solomon, 2005). The balance of ozone in the polar regions is influenced not only by radiative and chemical processes, but also by vertical and horizontal transport by the residual mean meridional circulation (e.g. Sabutis, 1997; Nikulin and Karpechko, 2005) and quasi-horizontal mixing processes in the mid-latitude regions (Chen et al., 1994; Müller et al., 2005), where tracer transport is dominated by wave breaking (Homeyer et al., 2011; Homeyer and Bowman, 2013). The EEP-induced changes in ozone concentration can potentially alter the temperature distribution and circulation throughout the stratosphere through a top-down mechanism (Kodera and Kuroda, 2002), with possible consequences in the troposphere. While it has been indicated that variations in UV irradiance during the 11-year solar cycle can modify stratospheric dynamics (Seppälä et al., 2013), the potential role of EEP on the dynamics of the stratosphere and troposphere is still debated. This is because of the complex interactions of the EEP forcing with ozone variability, which is driven by chemistry, radiation and dynamics, as well as planetary and gravity waves and their interactions with the mean-flow (Langford et al., 1996; Turunen et al., 2016).

Because the available observational record is limited it is problematic to attribute signals directly to GA in reanalysis datasets. Seppälä et al. (2013) found significant signals in polar stratospheric temperatures and zonal winds, especially during the solar maximum. Tomikawa (2017) also found differences attributable to GA in austral upper-stratospheric polar temperatures and wind in the Japanese 55-year Reanalysis, but only in July. However, it is unclear to what extent statistical significance, especially spatial significance, was properly assessed in those studies. Tartaglione et al. (2020) did not find any significant differences when applying a significance test that accounts for temporal and spatial correlations. In any case, the limited length of reanalysis records and paucity of selected GA events, combined with the internal variability of the atmosphere at these latitudes, makes a robust assessment of statistical significance an arduous task. It is also unclear whether the potential EEP-induced ozone or temperature signals would be imprinted in the reanalysis or not, given that the number of upper stratospheric temperature observations ingested during the reanalysis assimilation cycles is limited, and ozone is not fully interactive in most reanalysis systems.

It is possible to use a climate model to better address causality and potential mechanisms, and to quantify the potential effect of GA on climate variables, at least within the limited representations of dynamical and chemical processes and interactions of the model. Marsh et al. (2007) performed idealized experiments with the whole atmosphere community climate model (WACCM), contrasting a solar maximum and high GA with a solar minimum and low GA under time-invariant forcings. They found statistically significant, small (5–10%) stratospheric ozone variations in response to EEP forcing. Cullens et al. (2016) also compared a solar maximum with high GA to a solar minimum with low GA under steady conditions using the WACCM and found a dipole of polar temperature anomalies in the mesosphere and stratosphere in austral winter and spring. They suggested that these anomalies, characterized by a warm mesosphere and a cold stratosphere, were caused by the differences in the mean meridional circulation driven by changes in the gravity wave drag, which itself was associated with zonal wind changes. The WACCM sensitivity was examined by Peck et al. (2015), who compared the response of the WACCM4 with the WACCM3 in a similar set-up of a solar maximum with high GA versus a solar minimum with low GA. They found that the WACCM4 simulated a larger change in chemical species like odd nitrogen (NOy) and ozone, but no large differences between the two WACCM versions emerged in terms of temperature and wind.

Motivated by these studies, we investigate the respective roles of solar spectral irradiance and GA in affecting ozone, NOx and temperature through numerical experiments with steady forcing using the WACCM. A higher solar spectral irradiance in the UV band produces more ozone by enhanced photolysis and increased heating, larger meridional temperature gradients and stronger polar stratospheric jets. Lu et al. (2008) and Seppälä et al. (2013) argued, based on reanalysis data, that the impact of GA is stronger during periods of high solar irradiance (SI) when the polar vortex is more intense, and more pronounced toward late winter. This would suggest that GA and SI may influence each other during late winter and early spring. Moreover, it may be important to distinguish the seasonal effects of GA and SI, as the former is expected to affect the atmosphere mainly in winter and spring (due to NOx production and descent), whereas the latter also acts in summer (when photolysis is strongest).

In this paper, we attempt to separate the effects of GA from those driven by SI. In particular, we seek to evaluate to what extent they interact, and whether the inferences obtained from reanalysis data in the literature are supported by idealized model simulations or not. To this end, we extend the analyses of Marsh et al. (2007), Cullens et al. (2016) and Peck et al. (2015) by examining responses to two levels of GA (weak and strong) separately under steady solar maximum or solar minimum conditions. Furthermore, we aim to move beyond the zonal-mean diagnostics of previous model studies by analyzing the stratospheric and tropospheric patterns of the responses to the forcings.

The paper is organized as follows. Section 2 describes the model simulations and the methodology of the statistical analysis, including significance criteria. Section 3 reports and discusses the results of the application of the two significance tests. Section 4 presents the conclusions with a brief discussion.

2. Methods

2.1. Model description

We conducted numerical simulations of the atmosphere with version 5.3 of the WACCM, a high-top extension of the community atmosphere model and part of the community Earth system model (CESM; at version 1.2). WACCM5 is essentially a combination of the chemistry of the WACCM4 (Marsh et al., 2013) with the tropospheric physics package of the CAM at version 5.3 (Neale and Coauthors, 2012). The vertical domain extends from the Earth's surface to 5.9×10^{-6} hPa (~145 km geometric height) and it is discretized on 70 vertical hybrid pressure levels. The horizontal discretization used for this work is on a regular longitude-latitude grid with spacing of 1.9° in latitude and 2.5° in longitude. The dynamical equations are solved with the finite-volume dynamical core (Lin and Rood, 1997). The neutral chemistry is based on the model for ozone and related chemical tracers (MOZART), which simulates chemical and physical processes occurring along all the atmosphere (Kinnison et al., 2007). The parameterization of the auroral oval is based on the work of Roble and Ridley (1987). The ionization mechanism is parameterized by means of an ion-pair production rate that is a function of the estimated power deposited in the polar region as

a function of the Kp index, which represents a quasi-logarithmic local index of the three-hourly range in geomagnetic activity relative to an assumed quiet-day curve for a single geomagnetic observatory site. This estimate is obtained from the following formula:

$$h_{power} = 16.82 \cdot e^{(0.32 \cdot Kp)} - 4.86$$

From this relation, an energy flux is calculated, assuming that the auroral electrons have a Maxwellian energy distribution with a fixed characteristic energy of 2 keV. This results in an energy deposition confined to the lower thermosphere, with a peak at 110 km. The effects of the precipitation of higher energy electrons (>30 keV), which originate from the radiation belts and can sporadically penetrate into the mesosphere (Smith-Johnsen et al., 2018) are not represented in our simulations.

Four simulations with different solar and geomagnetic forcing terms were performed, namely H3, L3, H7 and L7 (cf Table 1). In each of these, solar and geomagnetic forcing terms were kept constant in time throughout the run. The designations H and L represent persisted high and persisted low solar forcing, respectively. The numbers 3 and 7 indicate persistent low GA and persistent high GA, to reflect the notional GA values of Kp 3 and 7, respectively.

Concerning solar forcing, the prescribed total SI and the spectral SI values were obtained from the observations of solar minimum conditions in the year 1996 (experiments denoted as L), and solar maximum conditions in the year 2000 (experiments denoted as H).

The f10.7 index, which is a measurement of the total emissions at a wavelength of 10.7 cm from all sources present on the solar disk and represents a satisfactory proxy of UV irradiance from the sun (Tapping, 2013), has a value of 210 (10^{22} J s^{-1} m^{-2} Hz^{-1}) for high solar activity (experiment H3 and H7) and a value of 70 (10^{22} J s^{-1} m^{-2} Hz^{-1}) for low solar activity (experiments L3 and L7). Our choice of the relatively extreme, but still realistic, values for the Kp and f10.7 indices are very similar to those in the steady WACCM experiments of Cullens et al. (2016) and Peck et al. (2015), and consistent with recommendations from NOAA (https://www.ngdc.noaa.gov/stp/GEOMAG/kp_ap.html).

We ran each experiment for 40 years; the first 5 years were considered spin up and not used in the analysis. The following 35 years were used in the analysis comparing one couple of experiments at a time.

To isolate the relative effects of GA and SI, a few additional simplifications were made. No solar proton events were considered in the experiments. The sea surface temperatures were prescribed with a repeated annual cycle matching present-day climatology. Similarly, a fixed quasi biennial oscillation cycle was prescribed. No volcanic forcing was used and no trend in greenhouse gases or ozone depletion species were imposed.

2.2. Statistical analysis and score definition

The significance of seasonal differences between two experiments, for example H3-L3, was assessed by a two-step statistical test. First, a permutation test (e.g. Wigley and Santer, 1990) was employed to estimate the statistical significance, at 5%, of the difference at each single point in the domain. In the second step, the effect on a larger scale was evaluated by computing the number of grid points with significant difference in a chosen domain. The rank of this number in a distribution of 5000 of such numbers was then evaluated with a Monte Carlo test.

To perform the permutation test the two 35-year-long samples from the two simulations were pooled together. Then, a resampling without replacement was made by arbitrarily assigning 35 years to one experiment and 35 years to the other. Such a resampling ensured that each of the individual 70 years was represented only once, in one of the two samples of 35 years (Wilks, 2006). Finally, we computed a new difference field. This procedure was then repeated 10,000 times, allowing us to build a sufficiently large distribution to evaluate the significance of the original difference field. A p-value of 0.05 defined the significance level for a two-tailed test distribution. However, this did not complete the statistical test for the difference field, since treating many spatial points simultaneously produces the problem of multiplicity, meaning that there is a non-zero probability of finding a significant result by chance (von Storch, 1982). Furthermore, when setting the significance level at 5%, a sample size of 13,824 points, (i.e. the number of horizontal grid points of the WACCM), provides as many as 700 significant results by chance. This is a common and often neglected problem in spatial statistics (Katz and Brown, 1991; Wilks, 2016). The null hypothesis assumes there is no difference between two experiments when the number of significant points in the difference field of a given variable is within the 5% confidence interval. Two possible ways to overcome the problem of multiplicity are the reduction of the p-value or the use of a Monte Carlo technique.

Monte Carlo simulations were performed employing a similar technique used to assess the significance of the single points. By pooling together the 70 years of the original experiments, 5000 experiment pairs were obtained. After they were randomly extracted they were assigned to the first or second experiment, creating a new couple of experiments for analysis. The numbers of statistically significant points in the resampling were hence collected together to build a statistical distribution. The score was defined by the percentile rank of the number of statistically significant points of the original difference field within that statistical distribution. The higher the rank in the distribution, the lower the probability that the number of statistically significant points was obtained by chance, which would indicate a possible effect of GA. A similar approach was used by Maliniemi et al. (2014) in a study on the relationship between northern hemisphere (NH) surface temperatures and the solar cycle. In our analysis, a score of 95 or higher is considered significant, while we refer to a score of 90 as marginally significant.

To understand the respective roles of SI and GA forcings on atmospheric dynamics, we analyze the differences between pairs of experiments, in terms of seasonally averaged zonal wind, temperature and diagnostics associated with the transformed Eulerian mean framework, namely Eliassen-Palm fluxes and residual circulation components (Edmon et al., 1980).

Table 1
Summary of experiments.

Experiment	Kp	Ap	SI year	F10.7 x (10^{22} J s^{-1} m^{-2} Hz^{-1})
H7	7	132	2000	210
H3	3	15	2000	210
L7	7	132	1996	70
L3	3	15	1996	70

3. Comparison of model spatial fields

This section presents a statistical analysis of the difference in NOx, ozone and temperature between experiment pairs to evaluate the spatial effect of GA and SI. These differences are presented either averaged over the total stratospheric column or at specific pressure levels. More specifically, the NOx and ozone stratospheric columns were computed by averaging vertically over all stratospheric levels from the stratopause (1 hPa) down to the tropopause, approximately defined here as 100 hPa at the equator, decreasing linearly to 200 hPa in the polar regions. The differences in the NOx column largely represents the overall NOx changes in the upper stratosphere, as there is little NOx in the lower stratosphere. In contrast, the stratospheric column ozone measured in Dobson units is strongly weighted by ozone in the lower stratosphere. In all the figures that illustrate differences between two experiments, dotted areas are statistically significant at 5% as defined by a permutation test.

Contrasting the pair of experiments H7 and L3, we first examine the difference in the model response between high SI/GA and low SI/GA, as in Marsh et al. (2007), Cullens et al. (2016) and Peck et al. (2015). We next contrasted the two experiments with high or low GA under the solar

minimum (L7 and L3). These experiments under the solar minimum conditions are vital to evaluate the role of GA in the model, as the SI may have positive or negative feedback with GA, as suggested by Lu et al. (2007). Finally, we examine the effect of SI under low GA by contrasting the two experiments H3 and L3.

We analyze mainly the differences of the seasonal means (December, January and February – DJF; March, April and May – MAM; June, July and August – JJA; and September, October and November –SON).

3.1. Joint influence of high geomagnetic activity and high solar irradiance (experiment H7-L3)

Fig. 1 illustrates the stratospheric NOx difference between experiments H7 and L3. In the SH, the difference scores are 100 in JJA and SON (austral winter and spring) and 99 in DJF (austral summer), indicating that the combined effects of SI and GA heavily influence the NOx abundance in the stratosphere. In the NH, the statistically significant points cover a much smaller area compared to the SH, and boreal winter (DJF) is the only season that registers a statistically significant impact. During MAM, the analysis reveals only a marginally significant difference. No significant impact is observed in the other two seasons.

Regarding ozone, Fig. 2 depicts that in the SH polar regions high SI and GA significantly reduce the stratospheric column ozone during spring (SON) – as may be expected from the catalytic ozone depletion due to an elevated NOx abundance – and that, while the deficit persists into summer (DJF) and autumn (MAM), it is no longer significant. There is also a marginal column ozone deficit during winter (JJA, i.e., during the polar night), which can only be explained by the circulation differences. The decrease of the averaged ozone column by up to 10 Dobson units during spring aligns with the findings of Marsh et al. (2007). Fig. 2c and d also clearly display the increased production of ozone in the tropical regions and its poleward transport. Table 2 further shows the polar-averaged scores for ozone at 2 hPa and 10 hPa. Statistically significant differences are found at 2 hPa for all seasons, and at 10 hPa during austral spring and summer. In the NH, the ozone column difference is notably positive (Fig. 2), hence opposite to what might be expected from the (weak) elevated NOx abundances, but this effect is only significant in boreal autumn (SON) with a score of 98. Fig. 2 depicts the excess in column ozone produced at lower latitudes and transported to the polar regions, and suggests that these production and transport processes have a greater efficacy than in the SH. The ozone differences in the polar regions at 2 hPa are statistically significant only during boreal summer and autumn, and at 10 hPa only in boreal summer (Table 2).

Concerning temperatures, Figs 3 and 4 convey the differences at 0.1 hPa and 500 hPa, respectively. The temperature differences in the mesosphere reveal significant scores in the SH for all seasons, which is in stark contrast to the insignificant temperature differences below that level (see Table 2, e.g., at 10, 200 or 500 hPa). An exception is the temperature difference at 500 hPa in austral autumn (MAM), which yields a significant score. In the NH, it is only during boreal summer (JJA) that the mesospheric temperature difference is statistically significant, at least in the polar-cap average. This is likely related to the higher SI having a more pronounced impact during summer, it is confirmed at 10 hPa, but not in the troposphere (Table 2) where only the temperature difference at 500 hPa in boreal winter (DJF) has a marginal impact score.

3.2. Geomagnetic activity under solar minimum condition (experiments L7-L3)

Fig. 5 depicts the stratospheric NOx difference between experiments L7 and L3. In the SH, the stronger GA in L7 produces more NOx than in L3, and the difference is statistically significant for all seasons. Comparing Fig. 5 with Fig. 1 reveals that the effect of GA on NOx in the SH is stronger in L7 than in H7, especially at middle and low latitudes. The scores are higher and the spatial extension is larger. In the NH, the stratospheric NOx differences are statistically significant only in boreal spring (MAM), and only marginally significant in boreal winter (DJF). A further comparison of Fig. 5 with Fig. 1 reveals that the enhanced photolysis of NOx due to high SI on stratospheric NOx at low and middle

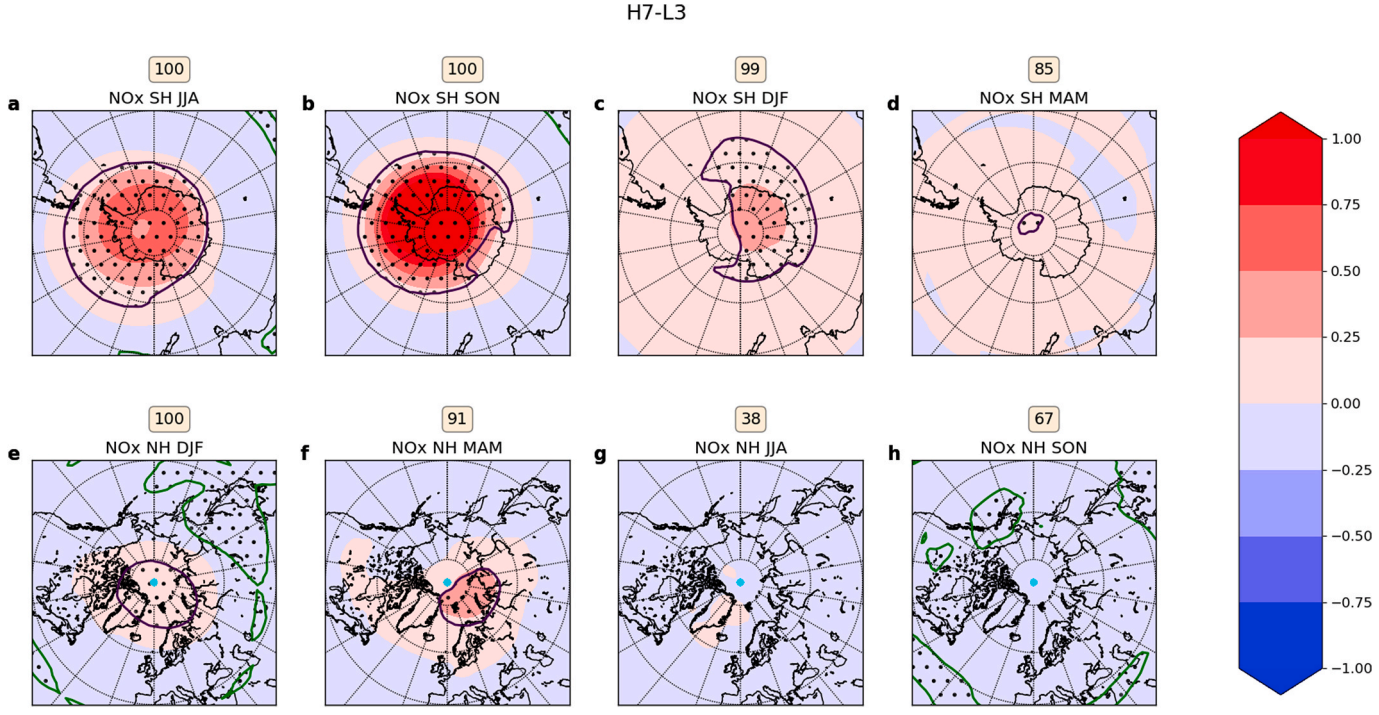

Fig. 1. Stratospheric NOx difference, H7-L3. Values are in number of 10^{15} molecules cm^{-2}. The dots indicate statistically significant points. The purple lines surround statistically significant positive values; the green lines surround statistically significant negative values. The number over each panel indicates the percentile rank of the statistical test over the polar region.

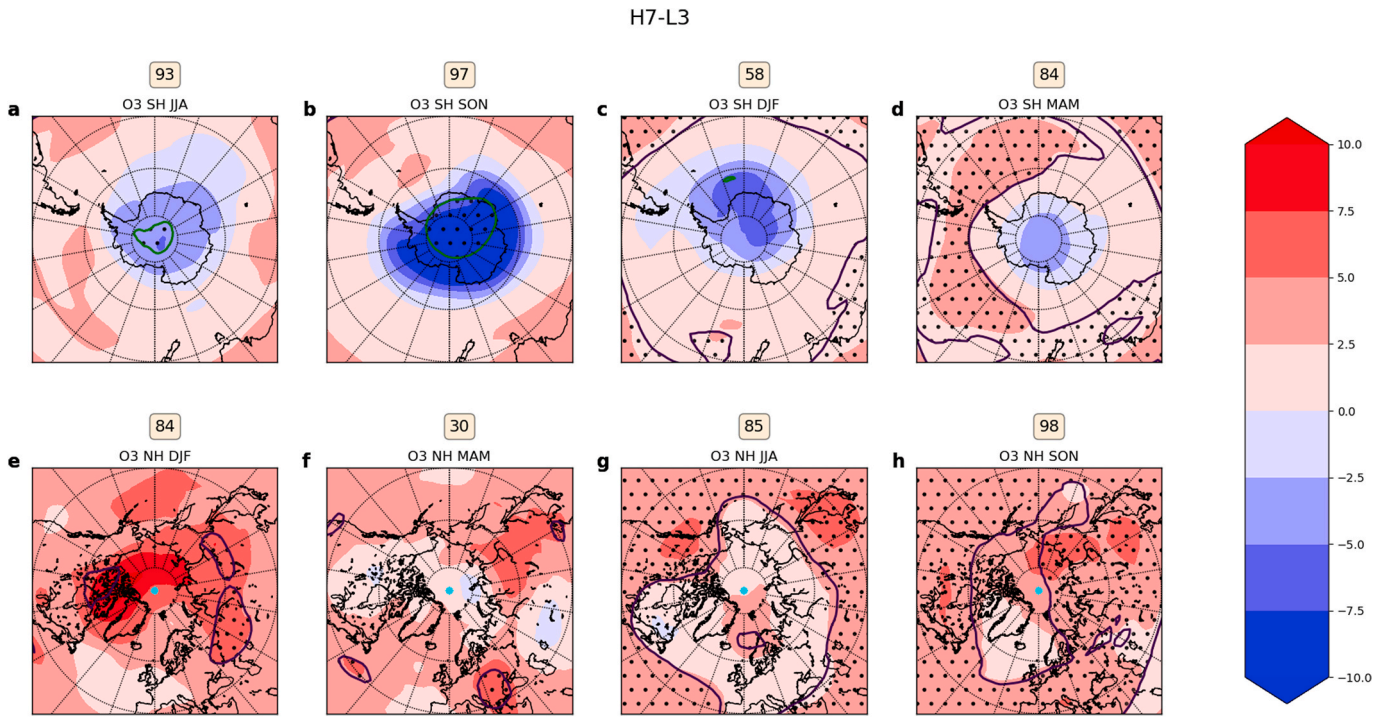

Fig. 2. As Fig. 1, but for stratospheric ozone difference, H7-L3. Values are in Dobson units.

Table 2
Rank reached by some difference fields obtained with H7 and L3 experiments of a few variables in the test of multiplicity for the polar regions (60°–90°) at different levels. The label "Strato" means that the variable is vertically averaged in the stratosphere. In bold are the values larger than or equal to the 95th percentile; in italics are those between the 90th and 95th percentiles.

Variable	Level	MAM		JJA		SON		DJF	
		SH	NH	SH	NH	SH	NH	SH	NH
NO_x	Strato	85	*91*	**100**	38	**100**	67	**99**	**100**
O_3	Strato	84	30	*93*	85	**97**	**98**	58	84
O_3	2 hPa	**100**	63	**100**	**100**	**100**	**96**	**100**	14
O_3	10 hPa	87	50	28	**100**	**100**	71	**100**	24
T	0.1 hPa	**100**	80	**97**	**100**	**97**	68	*94*	24
T	10 hPa	83	23	74	**100**	71	25	80	25
T	200 hPa	73	23	43	63	87	9	36	27
T	500 hPa	**98**	24	59	84	54	60	32	**95**

latitudes outweighs the effect of the increased GA.

The difference between experiments L7 and L3 (Fig. 6) also elucidates that, in the SH, the ozone column only significantly decreased during austral winter and spring. This significance is also seen at 2 hPa and further down at 10 hPa in spring (Table 3). In contrast to the high SI case, ozone reduction in L7 is predominantly at high latitudes, with no notable positive differences at mid and low latitudes. In the NH, there are no significant differences in column ozone in any season, but there is a significant ozone signal at 2 hPa during boreal spring and summer. Comparing Fig. 6 with Fig. 2 reveals that SI causes a more significant change in ozone (in boreal autumn at middle and low latitudes) than GA.

Regarding temperature, Table 3 presents no significant scores at any levels and only a marginally significant effect at 0.1 hPa during austral winter and spring in the SH. In summary under low SI, GA has a notable effect on NOx in both the SH and NH, some impact on ozone in the SH, but no significant effect on temperature during the solar cycle minimum on stratospheric and tropospheric pressure levels.

3.3. *Influence of solar irradiance under low geomagnetic activity (experiments H3-L3)*

Fig. 7 illustrates the stratospheric NOx difference between the experiments H3 and L3. In both hemispheres, nearly all seasons show statistically significant negative differences (see also Table 4), implying that SI tends to reduce NOx not only at midlatitudes due to stronger photolysis, but also in the polar regions, except in winter. The high latitude NOx decrease is not significant in NH summer. This high latitude decrease in NOx must be contrasted with the NOx increase due to GA as described in Sections 3.1 and 3.2 and the decrease may be due to the combined effects of enhanced NOx production and transport from lower latitudes. Similarly, there is a reduction in the SH polar region (Fig. 8) which is only significant in SON. NOx and ozone share similar patterns of reduction from winter to summer, sometimes covering the entire polar cap, from −60° to the poles, which indicates that the ozone deficit is not caused by the NOx-induced catalytic loss (an ozone deficit would have to correspond to a NOx enhancement), but rather by the change in transport. The column ozone differences are significantly positive only in the NH during autumn. Again, this may reflect higher summer-time production of ozone in the middle and low latitudes and its subsequent poleward transport. The temperature differences (Table 4) are significant in the mesosphere in the SH for all seasons, and in winter and summer at 10 hPa. In the NH they are significant in the mesosphere in summer and marginally significant in autumn.

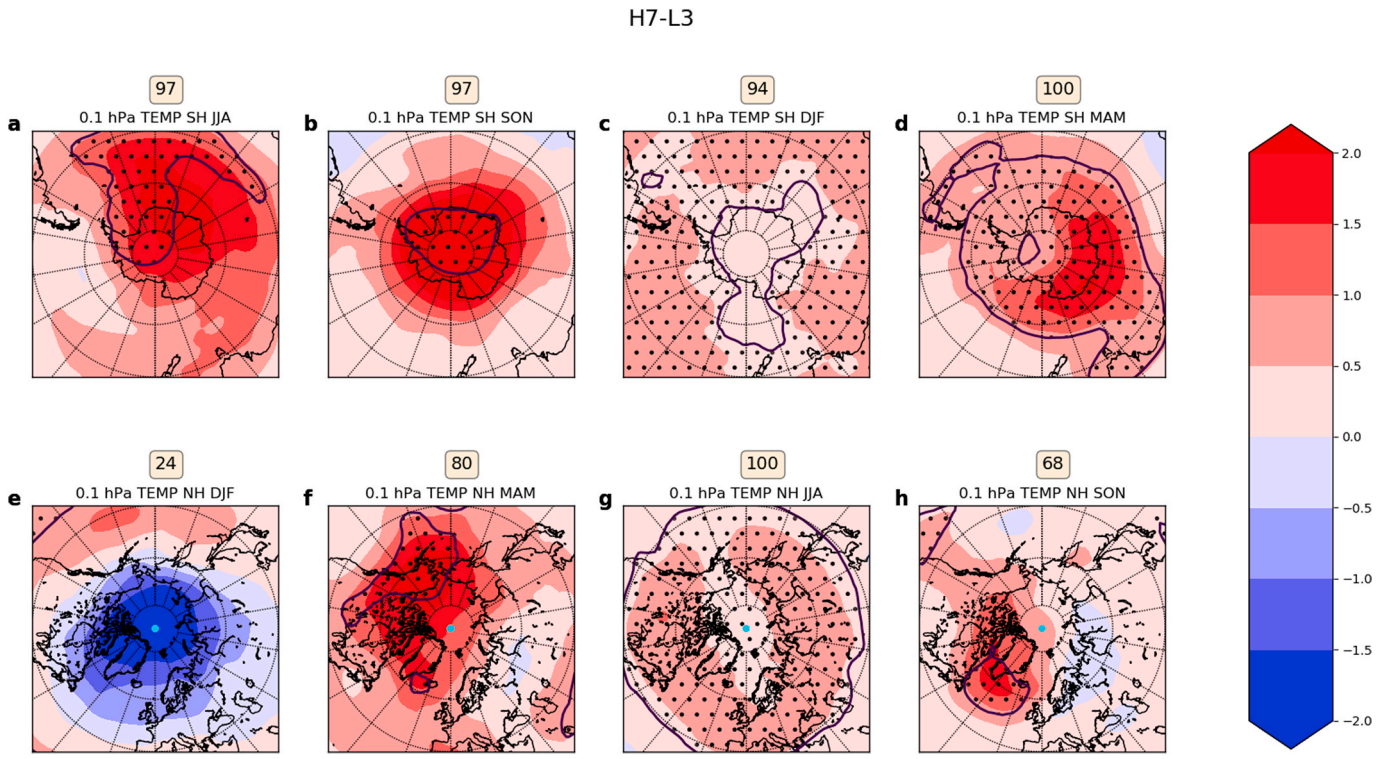

Fig. 3. As Fig. 1, but for 0.1 hPa temperature difference, H7-L3. Values are in K.

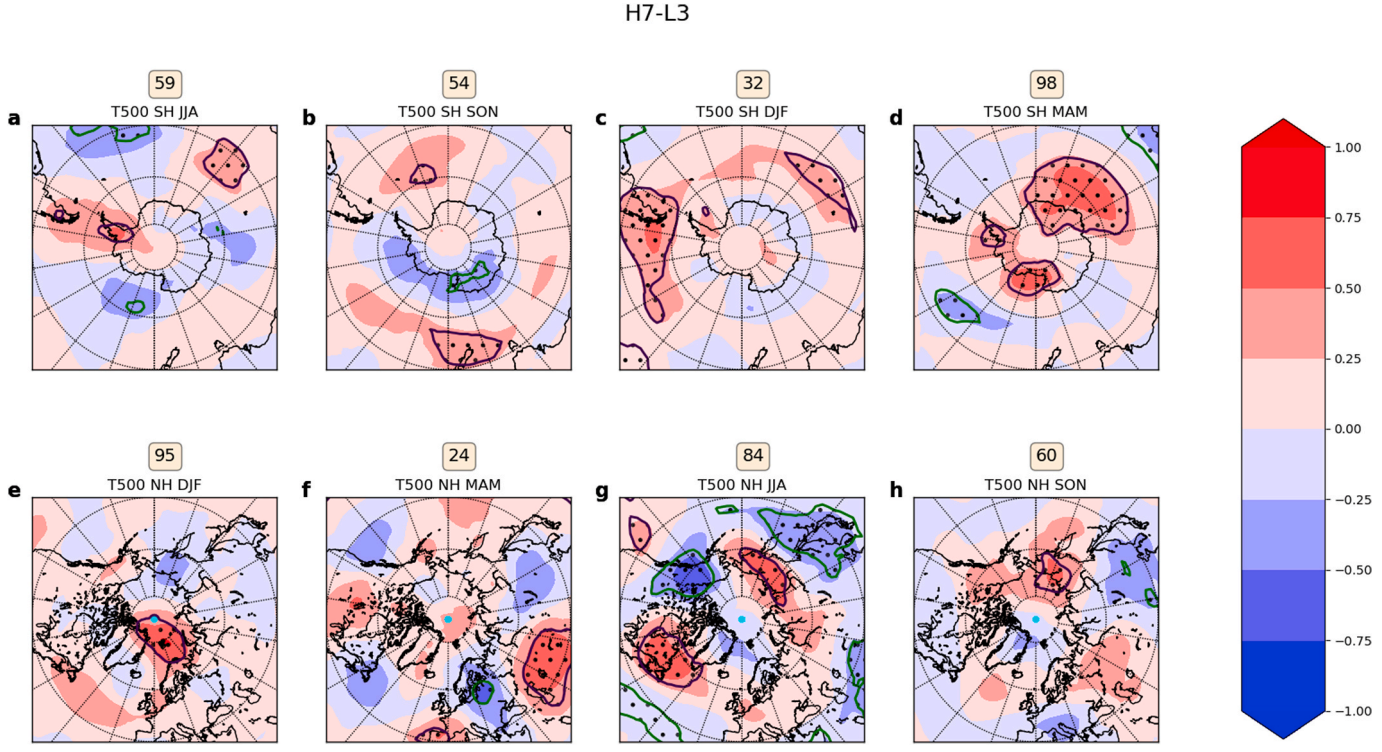

Fig. 4. As Fig. 1, but for 500 hPa temperature difference, H7-L3. Values are in K.

3.4. *Vertical distribution of monthly averages in the southern polar region*

Fig. 9 depicts time-height cross-sections of monthly averaged differences of NOx, ozone, and temperature for the H7-L3 case. NOx is enhanced in the lower mesosphere and upper stratosphere (Fig. 9a) and descends from the upper stratosphere to the lower stratosphere in the spring, while ozone shows a deficit below 1 hPa (Fig. 9b). The temperature difference (Fig. 9c) reveals a vertical dipole with higher temperatures in the lower mesosphere and lower temperatures in the middle and lower stratosphere. The negative ozone difference is located between the positive and negative temperature differences. These temperature changes are not consistent with the effect of ozone on long-

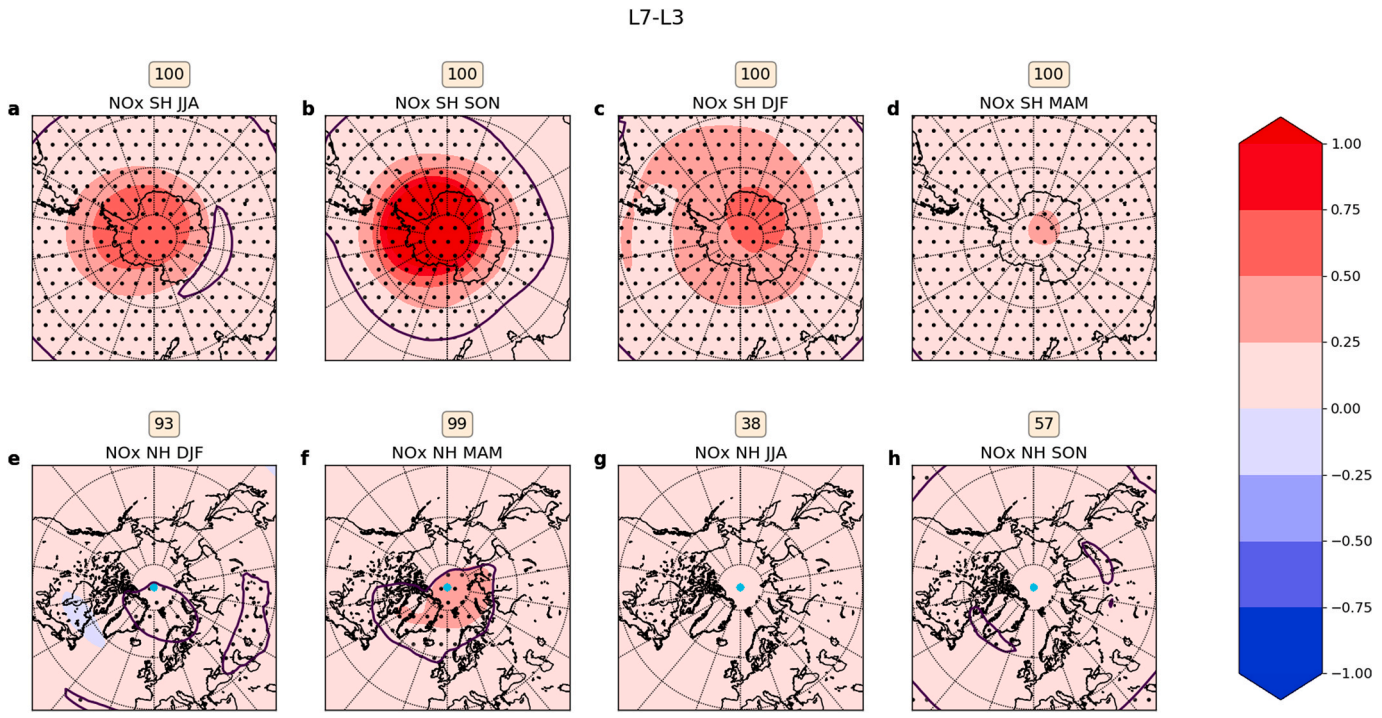

Fig. 5. As Fig. 1, but for stratospheric NOx difference, L7-L3. Values are in 10^{15} molecules cm^{-2}.

Table 3
As Table 2, but for L7-L3 experiment.

Variable	Level	MAM		JJA		SON		DJF	
		SH	NH	SH	NH	SH	NH	SH	NH
NO_x	Strato	**100**	**99**	**100**	38	**100**	57	**100**	*93*
O_3	Strato	28	24	**98**	24	**95**	17	24	21
O_3	2 hPa	32	**95**	**100**	**100**	**100**	15	67	60
O_3	10 hPa	*92*	13	79	60	**100**	16	**100**	13
T	0.1 hPa	16	24	*90*	35	*90*	23	51	26
T	10 hPa	74	24	26	26	72	24	21	24
T	200 hPa	20	19	48	51	68	66	31	17
T	500 hPa	71	28	34	77	26	70	6	7

wave radiative cooling, since the ozone decrease would then be collocated with a warm anomaly (Langematz et al., 2003). Rather these polar temperature changes are likely related to changes in the mean meridional circulation, as assessed in the next section.

GA effects at low SI (L7-L3 differences, Fig. 10) on NOx, ozone and temperature are similar to those found in the H7-L3 case (Fig. 9), but the temperature signal is not significant (Fig. 10c).

The SI effects at low GA (H3-L3) shown in Fig. 11 suggest a weak enhancement of polar NOx (Fig. 11a; note the small range of values compared to Fig. 9a or 10a). This NOx difference is still significantly different from ozone and temperature. Although GA is weak, there remains a small production of NOx in the late winter lower mesosphere that must be explained by the difference in SI (Fig. 11a), which drives higher NOx production in the mesosphere that descends into the stratosphere afterwards. The NOx-depleted region in the stratosphere, instead, is related to the higher production of ozone (Fig. 11 b) and it is another consequence of stronger SI. The SI effect on temperature is much higher than in the other cases, with the temperature differences (Fig. 11c) being greater and longer-lasting than those in the H7-L3 case, likely due to a combination of radiation and changes in the mean meridional circulation.

3.5. Discussion on dynamics

The preceding analysis reveals large temperature differences in the polar mesosphere and stratosphere that cannot be explained by radiative effects alone (e.g., Figs. 9 and 11). Previous studies (Kodera and Kuroda, 2002) suggested that SI modulates the zonally averaged zonal wind in the upper stratosphere, and that this modulation propagates down to the lower stratosphere through wave-mean flow interaction and is associated with changes in the Brewer-Dobson (BD) circulation circulation. Cullens et al. (2016) also suggested that the zonal wind change modulates the gravity wave drag in the mesosphere, hence the pole-to-pole mesospheric mean meridional circulation. To explore these dynamical changes, we calculated diagnostics based on the Eliassen-Palm flux and the transformed Eulerian mean formalism under the hypothesis of quasi-geostrophic approximation (e.g., Edmon et al., 1980).

Considering first the differences between the H3 and L3 experiments, Fig. 12 illustrates the seasonally averaged differences in zonal-mean zonal wind, temperature, ozone, Eliassen–Palm flux divergence (EPFD), the gravity wave drag and the vertical and meridional components of the residual circulation.

The SI influence is most evident in the SH where a persistent statistically significant difference in zonal wind indicates a stronger polar vortex. It starts to appear in the mesosphere during MAM, strengthens during JJA and persists until SON, a result consistent with other studies

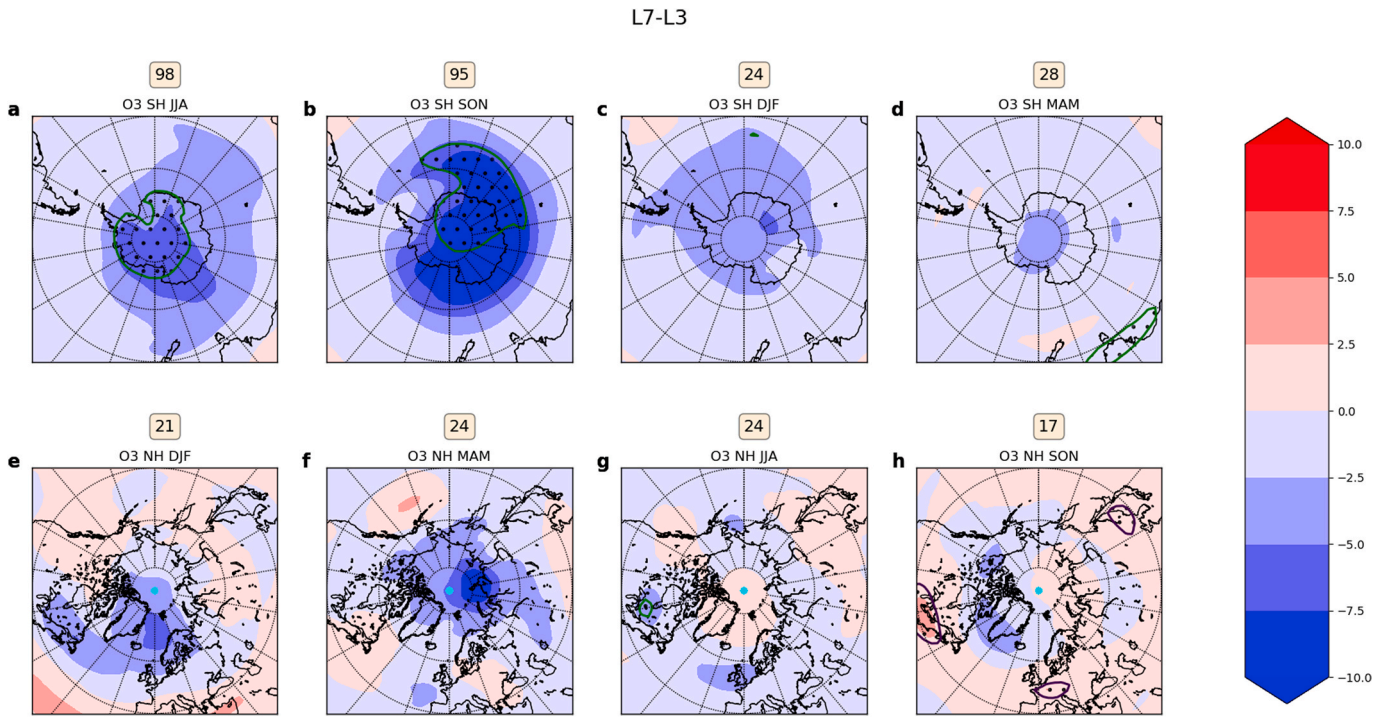

Fig. 6. As Fig. 1, but for stratospheric ozone difference, L7-L3. Values are in Dobson units.

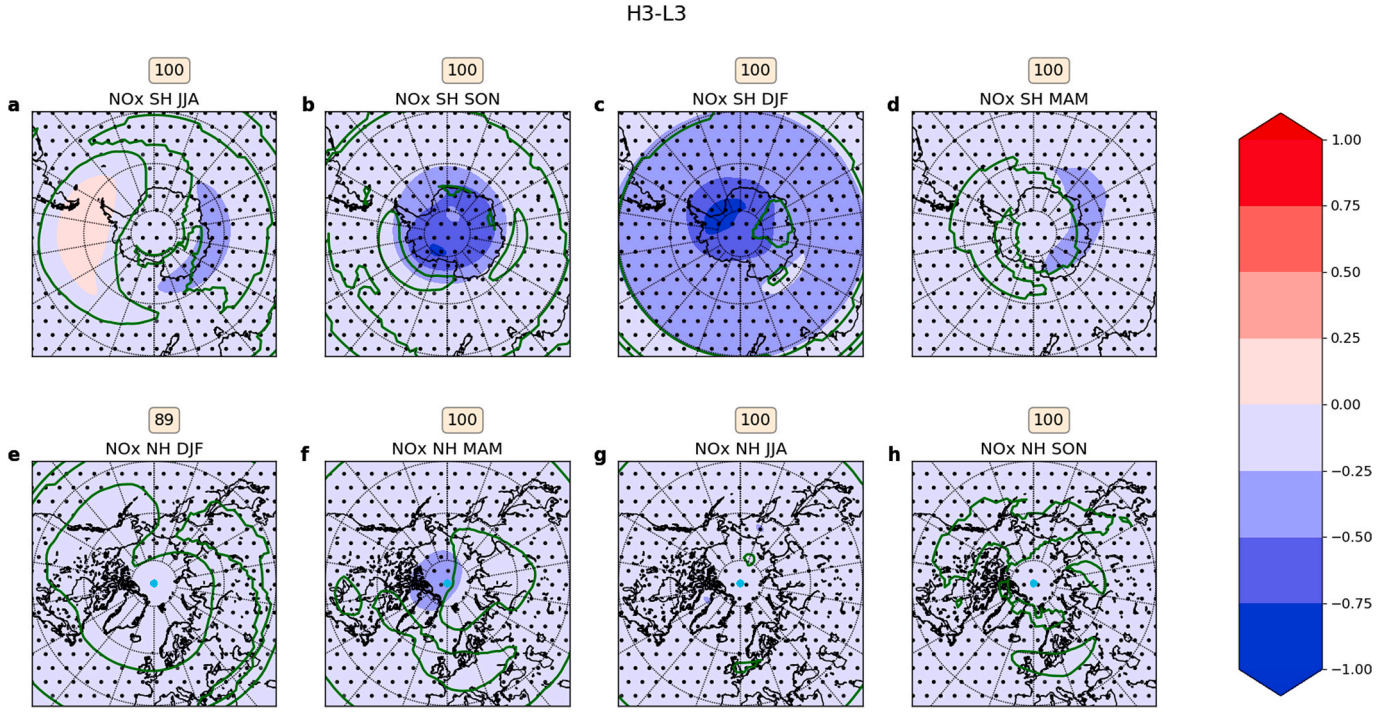

Fig. 7. As Fig. 1, but for stratospheric NOx difference, H3-L3. Values are in 10^{15} molecules cm^{-2}.

(Cullens et al., 2016; Kodera and Kuroda, 2002; Kuchar et al., 2015). This stronger vortex in the upper stratosphere should be considered a result of maintaining the thermal wind balance. In the mesosphere, the positive temperature anomaly is consistent with an enhanced descent (i.e., a negative anomaly in the vertical residual circulation in Fig. 12). In contrast, in the polar stratosphere the BD circulation is weakly reduced in JJA and SON (i.e., a positive anomaly in the vertical residual circulation in Fig. 12). A further indication of the weakened BD circulation is the colder lower stratosphere at high latitudes during those seasons. Reduced meridional transport due to the weakened BD circulation leads to a reduction of the winter and spring ozone amount in the polar region, which was also seen in Fig. 11c, though there could also be increased chemical ozone loss in the cold and isolated polar vortex (Schoeberl and Hartmann, 1991). The two processes interact, and distinguishing their relative contributions is not straightforward and requires dedicated simulations (Isaksen et al., 2012). Moreover, consistent with the reduced

Table 4
As Table 2, but for H3-L3 experiment.

Variable	Level	MAM		JJA		SON		DJF	
		SH	NH	SH	NH	SH	NH	SH	NH
NO_x	Strato	**100**	**100**	**100**	**100**	**100**	**100**	**100**	89
O_3	Strato	86	60	83	87	**98**	**97**	85	87
O_3	2 hPa	**98**	46	**98**	**100**	78	**100**	**100**	13
O_3	10 hPa	**95**	76	88	**100**	83	**99**	**100**	85
T	0.1 hPa	**100**	24	**100**	**100**	**97**	*92*	**99**	26
T	10 hPa	82	23	**100**	**100**	*92*	81	**100**	26
T	200 hPa	24	73	7	70	7	50	42	*91*
T	500 hPa	78	8	46	40	39	78	35	*90*

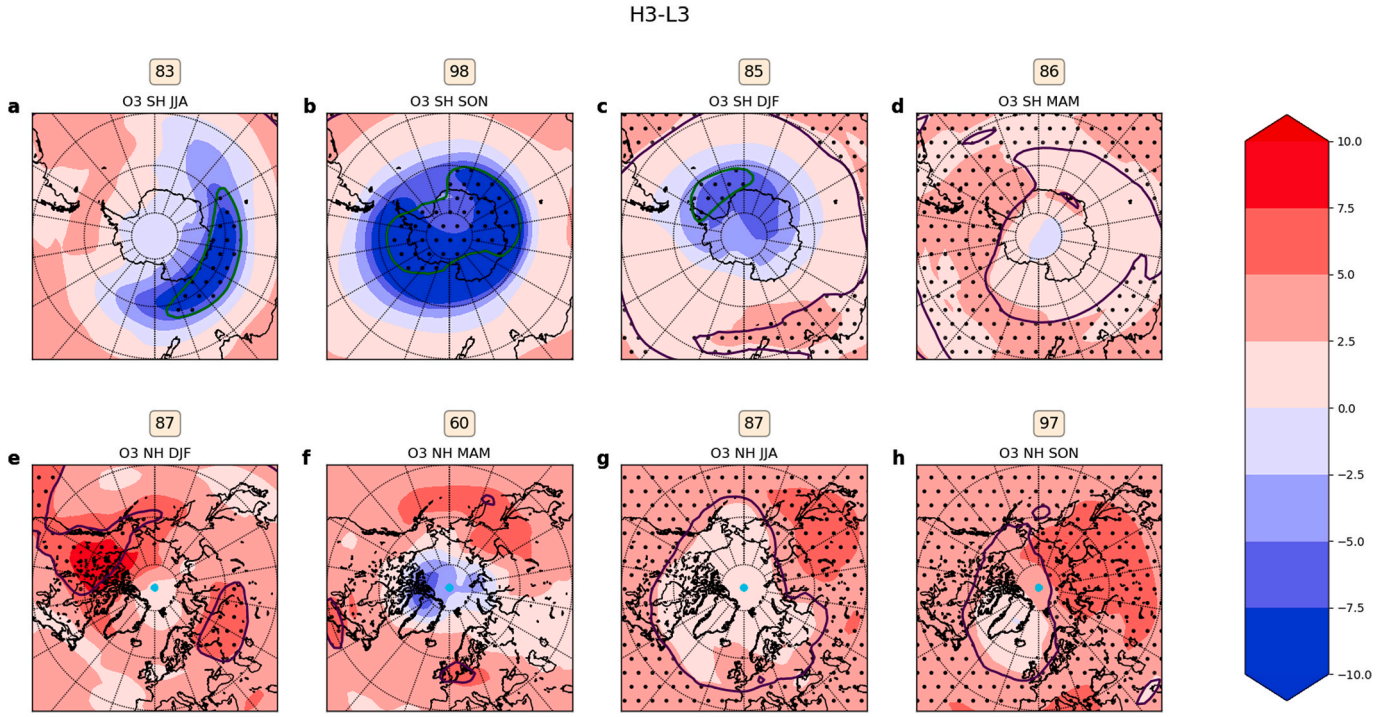

Fig. 8. As Fig. 1, but for stratospheric ozone difference, H3-L3. Values are in Dobson units.

BD circulation, the tropical stratosphere is warmer in H3 than L3, especially during JJA. To summarize, in the SH, the H3-L3 differences indicate a stronger polar vortex, an enhanced mesospheric mean meridional circulation and a weaker BD circulation consistent with the temperature anomalies in Fig. 11c.

In the NH, by contrast, the increase in zonal-mean zonal wind is not significant. A significant cold lower stratospheric polar anomaly is seen in spring, along with a warm anomaly aloft, but that cold anomaly does not persist into summer as is the case in the SH. The higher polar temperatures in the upper stratosphere in winter and spring are consistent with a strengthened BD circulation, as demonstrated by the enhanced poleward and downward velocities and the negative difference in lower stratospheric EPFD (Fig. 12).

The different zonal flow leads to differences in the gravity wave drag through stratospheric filtering (Fig. 12). Note that the gravity wave drag generally dominates over the EPFD in the mesosphere. while, in the stratosphere the EPFD tends to be more important. Our results are generally consistent with the findings of Cullens et al. (2016), who examined the SH response to solar forcing in WACCM with very similar parameters (solar max and high GA contrasted to solar min and low GA). The consistency between the large negative gravity wave drag difference caused by the enhanced westerlies below, and the descent and warm mesospheric temperature differences is indicative of a strengthening of the pole-to-pole mesospheric branch of the mean meridional circulation (Fig. 12). It also highlights the importance of the gravity wave drag changes in driving mesospheric temperature in our simulations.

Between H7 and L3 (Fig. 13), there is a statistically significant negative difference in zonal-mean zonal wind in the wintertime NH. This negative difference is not what is expected from the observational study of Kodera and Kuroda (2002), but winter zonal-mean zonal wind anomalies between solar maximum and solar minimum in the NH, where internal variability is large, have not been consistent in sign among different model studies or been statistically significant (Larkin et al., 2000; Peck et al., 2015).

In our simulations, the reduced NH winter polar vortex is associated with the effect of GA under high SI, which is stronger, and opposite in sign, to that found under low SI. A vertical dipole in polar temperature, characterized by a cold mesosphere and a warm stratosphere, is consistent with the anomalies in the vertical component of the residual circulation, e.g., anomalous mesospheric ascent driven by positive differences in EPFD, and anomalous stratospheric descent. Again the vortex decrease is associated with an opposite (positive) gravity wave drag that reinforces the effect of EPFD. In summary, there is a stronger BD circulation, accompanied by a reduction in the stratospheric westerlies and an increase in polar stratospheric ozone abundance, and a reduced pole-to-pole mean meridional circulation.

In the SH, the effects of GA under solar minimum conditions (L7-L3, Fig. 14) are similar, but weaker, than those of SI in the H3-L3 case

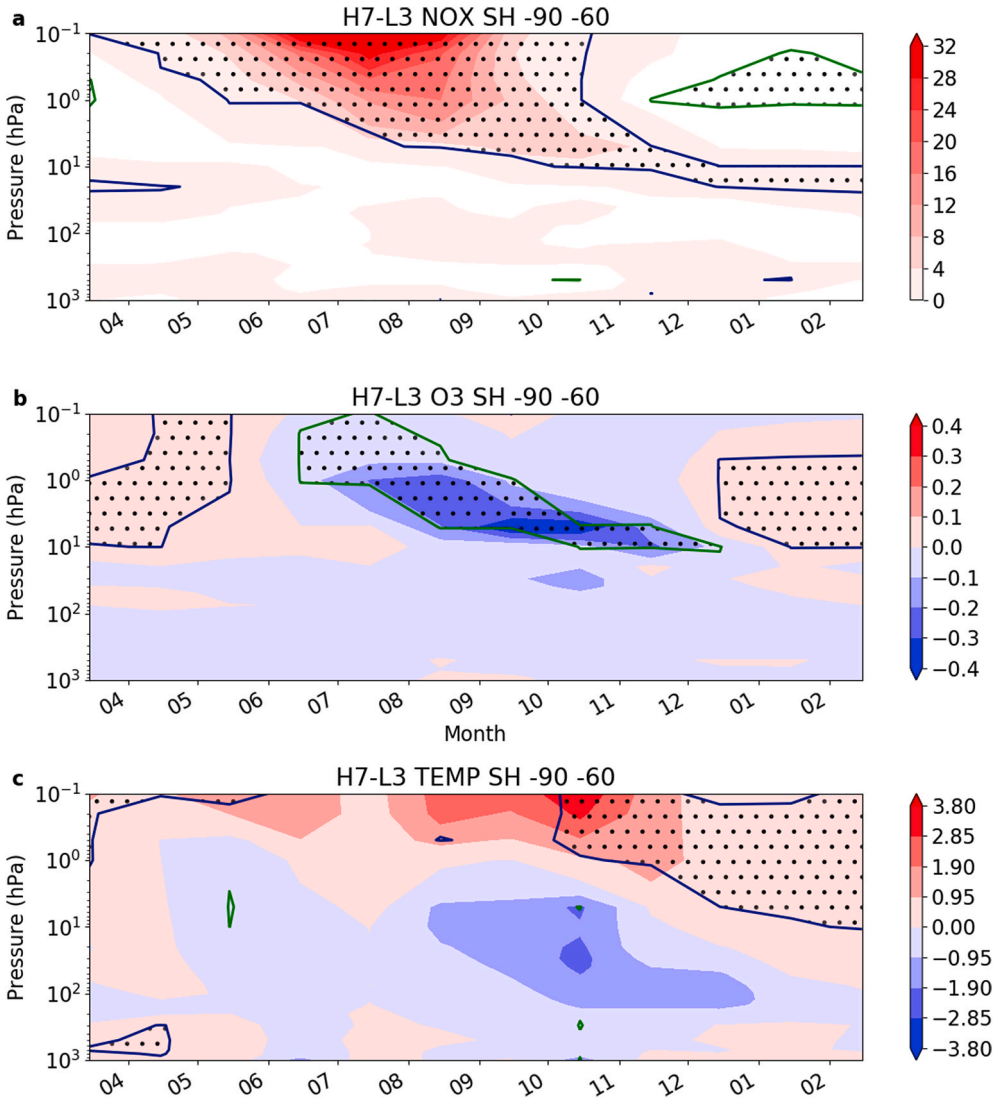

Fig. 9. Monthly average of NOx (a), O 3 (b), and temperature (b) differences (H7-L3 experiments) in polar cap (−60° -90°) of the Southern Hemisphere. The purple and green lines delimiting positive and negative dotted areas indicate that the differences are statistically significant with a permutation test. Differences are ppb for NOx, ppm for O 3, and K for temperature. White areas in the panel (a) indicate values between 0 and -1 ppb.

(Fig. 13). There is a stronger polar jet especially in austral spring, with a reduced BD circulation and stratospheric ozone. The impact in the NH is more limited than in the SH and the statistically significant differences appear to be confined to small areas. These results suggest that the influence of GA influence on NOx, ozone and temperature depends on SI conditions.

The effects of GA under SI maximum conditions H7-H3 (Fig. 15) are indeed different than under solar minimum conditions (Fig. 14). At mid-latitudes and in the polar region, especially during the winter season in the SH, SI produces higher amounts of ozone in upper levels of the atmosphere in H3 than H7. These high values of ozone block part of UV and prevent the production of ozone in the lower levels. The experiment H7, on the other hand, exhibits a reduction of ozone compared with H3 in the upper levels of the stratosphere because of the high amount of NOx coming from the mesosphere and more ozone production of at lower levels.

As in the previous cases, the temperature differences cannot be explained only in terms of radiative change (this is well visible in wintertime as there is no overlapping of ozone and temperature differences), but it are related to dynamical effects involving the residual circulation. The quadrupole in the SH temperature is associated to a corresponding quadrupole in the vertical component of the residual circulation, with colder temperatures where the vertical component is positive and vice versa. The lower temperature gradient between the equator and the SH mid-latitude produces a reduction of the zonal wind speed in the mid-latitude regions, a result that is opposite to that observed in H7-L3, where larger zonal wind speeds are observed at mid-latitudes (Fig. 13). The negative zonal wind difference around 60S in (H7-H3) indicates a weaker austral polar vortex consistent with a stronger BD, while cold mesospheric temperature differences are consistent with the anomaly in ascent.

In the NH winter, there is a similar behavior with a dipole in the temperature difference, as well as positive residual vertical velocity difference over the high-latitude region, a negative zonal wind difference, albeit weaker than in the SH. Corresponding to the stratospheric jet decrease, the gravity wave drag is now slightly enhanced (significantly in JJA) and the positive drag is associated with mesospheric ascent, as expected.

Compared with the L7-L3 experiment the difference fields exhibit many features that involve dynamical interactions and very large differences suggesting that the mutual interaction, when SI is high, can have nonlinear influence on the examined variables.

As a measure of non-linearity, we compare the difference H7-L3 with the combination (H3-L3)+(L7-L3). If the effects of SI and GA were

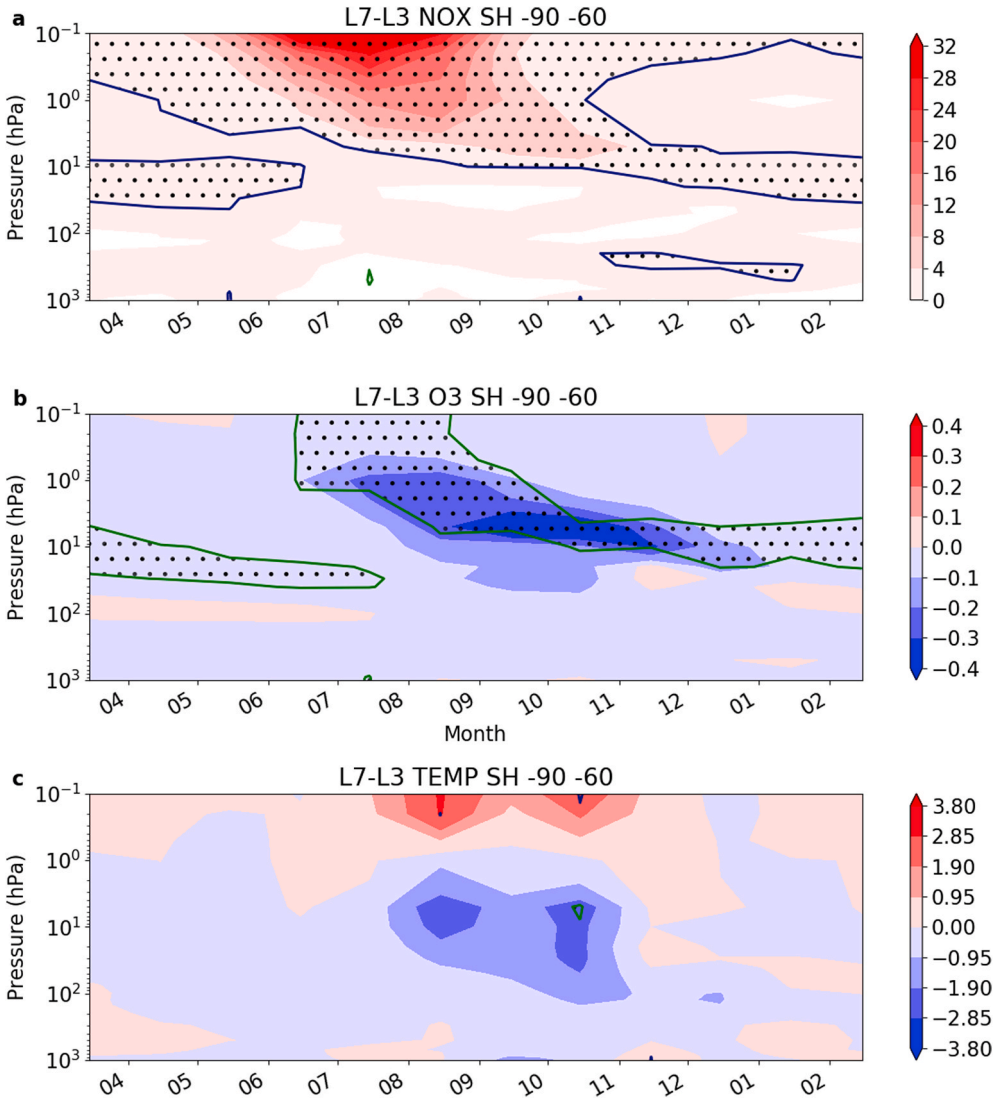

Fig. 10. As Fig. 9, but for experiment L7-L3.

independent of each other, then (H3-L3)+(L7-L3) should be nearly equal to H7-L3. Fig. 16 shows the 10 hPa temperature difference between the linearly added difference pairs (H3-L3)+(L7-L3) and the difference for the combined SI and GA effects (H7-L3), which may include nonlinearities.

In the SH there are a few seasons (JJA, SON and DJF) that show differences that are not statistically significant. The season MAM exhibits statistically significant differences. These results suggest that in the SH the interaction between SI and GA is linear or weakly nonlinear. The NH reveals a statistically significant difference between nonlinear and linear combinations in almost all the seasons, suggesting that the nonlinearity has a more profound presence in this hemisphere.

A further analysis of the detailed mechanisms behind the nonlinear interaction between SI and GA is certainly warranted, but is beyond the scope of this paper.

4. Conclusions

We present an assessment of the relative contributions of GA and SI to stratospheric climate anomalies based on numerical simulations with the WACCM with prescribed steady forcings. The model includes fully interactive atmospheric chemistry and we focus on the effects of different forcings on ozone, NOx, temperature and their statistical significance when compared with internal variability. To draw these conclusions we performed a two-fold statistical estimation; first, we employed a temporal permutation test that yields the statistical significance of single points in the domain, and second, we ran a Monte Carlo test that assesses the significance of the spatial effects on each variable.

Previous studies with the WACCM (e.g. Marsh et al., 2007; Peck et al., 2015; Cullens et al., 2016) have considered the concurrent impacts of GA and SI, as in our comparison between the H7 (high SI, high GA) and L3 (low SI, low GA) experiments. By comparing two other pairs of experiments, L7-L3 (GA effects only, at low SI) and H3-L3 (SI effects only, at low GA), we estimated the relative roles of GA and SI. Significant effects were found only in individual seasons, or at specific altitudes, or not at all.

Although further studies are needed to quantify the physical processes involved in the interaction between GA, SI and climate, our statistical analysis of these idealized experiments may be summarized in the following points:

1) GA strongly increases polar column NOx abundance in the SH, irrespective of SI, as this impact is visible in all seasons under the minimum solar condition (L7-L3 difference) and in most seasons under the maximum solar condition (H7-L3 difference). Stratospheric column ozone is also then notably reduced during the austral

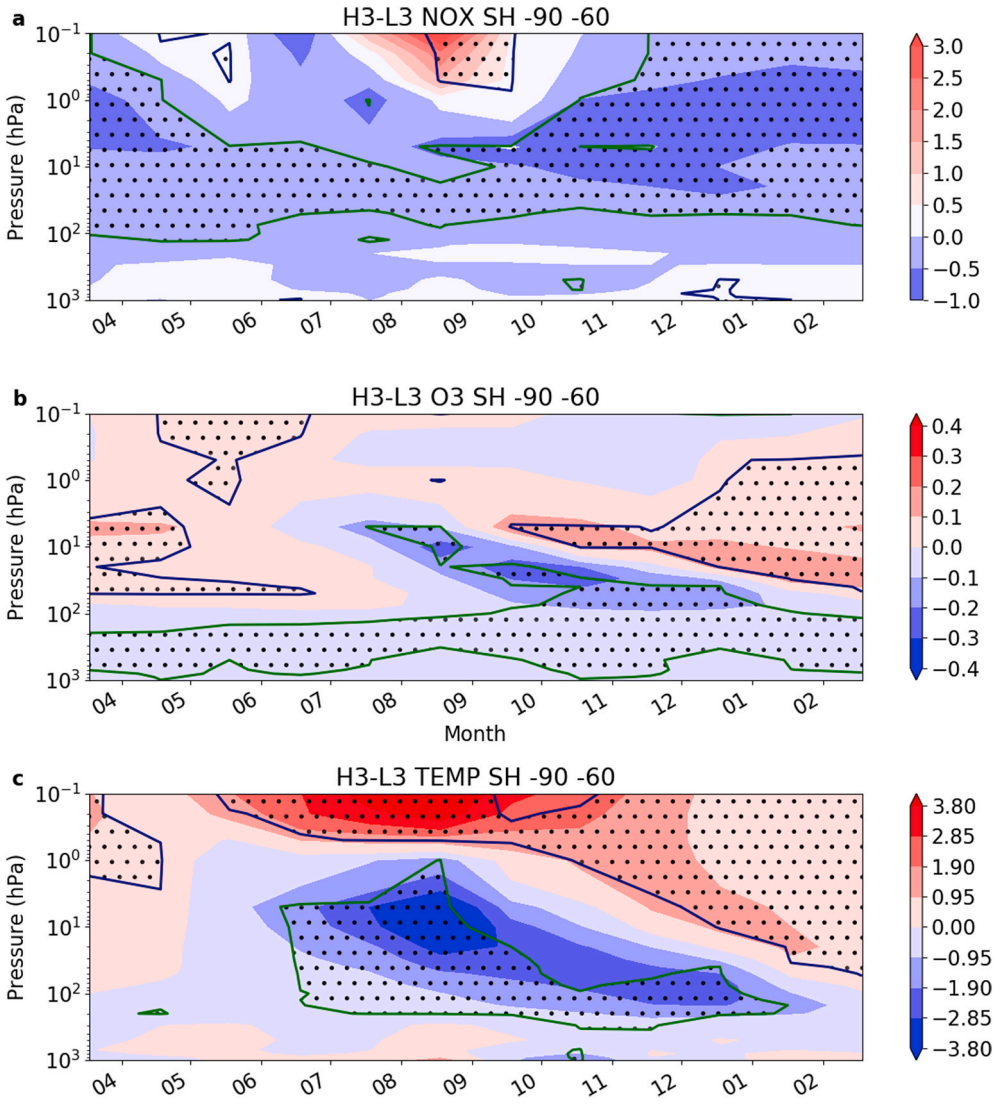

Fig. 11. Monthly average of NOx (a), O 3 (a), and temperature (b) differences (H3-L3 experiments) in polar cap (−60° -90°) of the Southern Hemisphere. The purple and green lines delimiting positive and negative dotted area indicate that the differences are statistically significant at 5% with a permutation test. For NOx, the value range is different from Figs. 9 and 10.

winter and spring. GA significantly alters the zonal-mean zonal wind and temperature and the BD circulation, especially in the SH, albeit less so than SI. However, the sign of effect of high GA depends on whether it occurs under solar maximum or solar minimum conditions. The GA effect on the horizontal temperature maps is generally limited. This result is consistent with that recently obtained by Meraner and Schmidt (2018) who found, using a 150 years simulation with the Max Planck Institute Earth system model, that EPP causes only small changes in the stratospheric circulation and temperature and has only a marginal effect on surface temperature.

2) SI has a significant impact on the ozone chemistry and on mesospheric and stratospheric temperatures, as clearly seen from the H3-L3 differences. When SI and GA are combined (e.g. in the H7-L3 difference), the higher spectral SI in the UV band has a positive effect on ozone production. This positive effect is larger than the ozone decrease that would be caused by additional production of mesospheric NOx associated with high GA. The higher ozone and temperature values in H7 and H3 are consequently due mainly to SI.
3) The comparison of the H7-L3 and L7-L3 differences indicates that there is a mutual interaction between SI and GA, which is in agreement with the conclusions of Lu et al. (2007). The interaction would seem almost linear (or weakly nonlinear) in SH and nonlinear in NH.

Moreover, the aforementioned results suggest that to understand the role of GA on the Earth's climate, it is important to factor in the effects of SI.

Prescribing a steady repeating cycle of sea-surface temperatures allow a better isolation of the possible top-down mechanisms, and our simulations appear to have sufficient duration (pairs of simulation with 35 years are compared) to allow a robust statistical estimation of significant changes attributable to solar forcing, in terms of SI and GA, in the SH. As found in previous studies (e.g., Kvissel et al., 2012; Tomikawa, 2017), most of the statistically significant changes are observed in the SH rather than the NH, where the higher natural stratospheric variability makes the effect of GA more difficult to detect and may require longer simulations.

Data and software availability

WACCM was downloaded by https://www2.acom.ucar.edu/gcm/waccm and adapted by NorESM group.

H3-L3

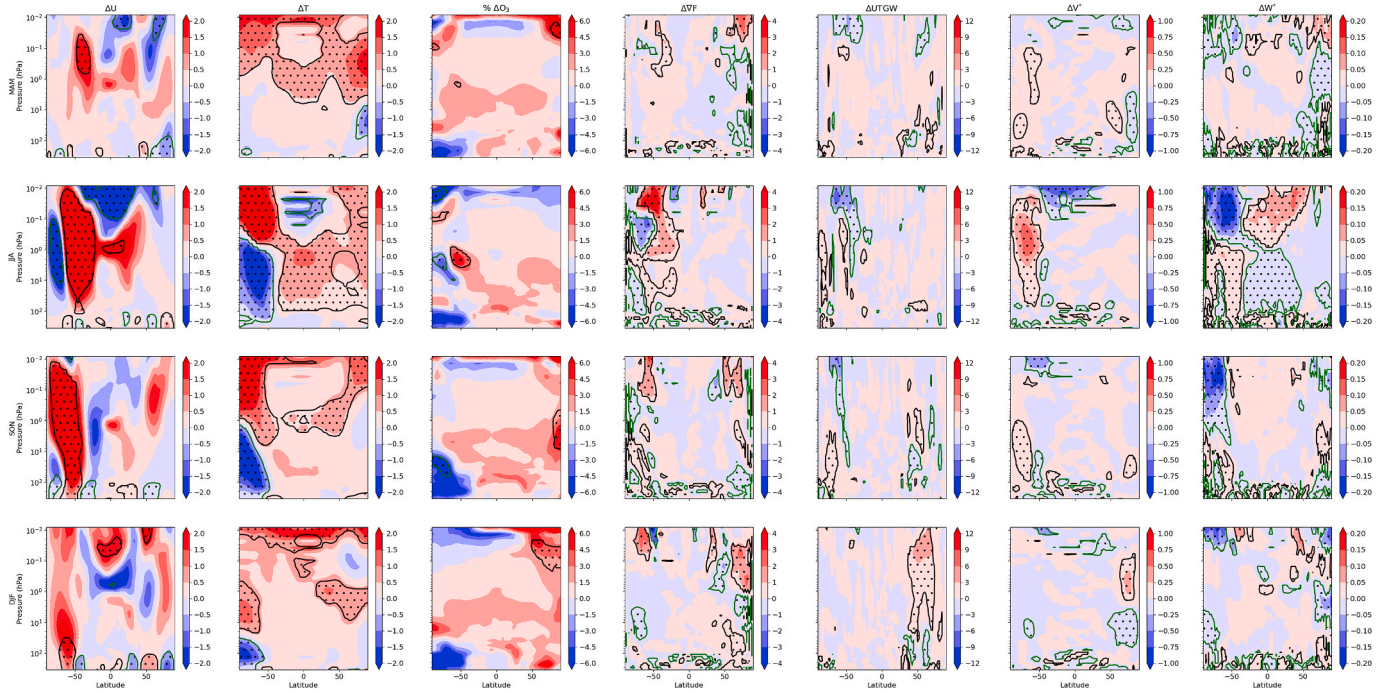

Fig. 12. The seasonally averaged differences H3-L3 in zonal-mean zonal wind (m s^{-1}) zonal-mean temperature (K), ozone (normalized on the seasonal mean, in percent), Eliassen-Palm flux divergence (m s^{-1} day^{-1}), gravity wave drag (m s^{-1} day^{-1}), meridional (m s^{-1}) and vertical (cm s^{-1}) components of the residual circulation. The black and green lines delimiting positive and negative dotted areas indicate that the differences are statistically significant at 5% with a permutation test.

H7-L3

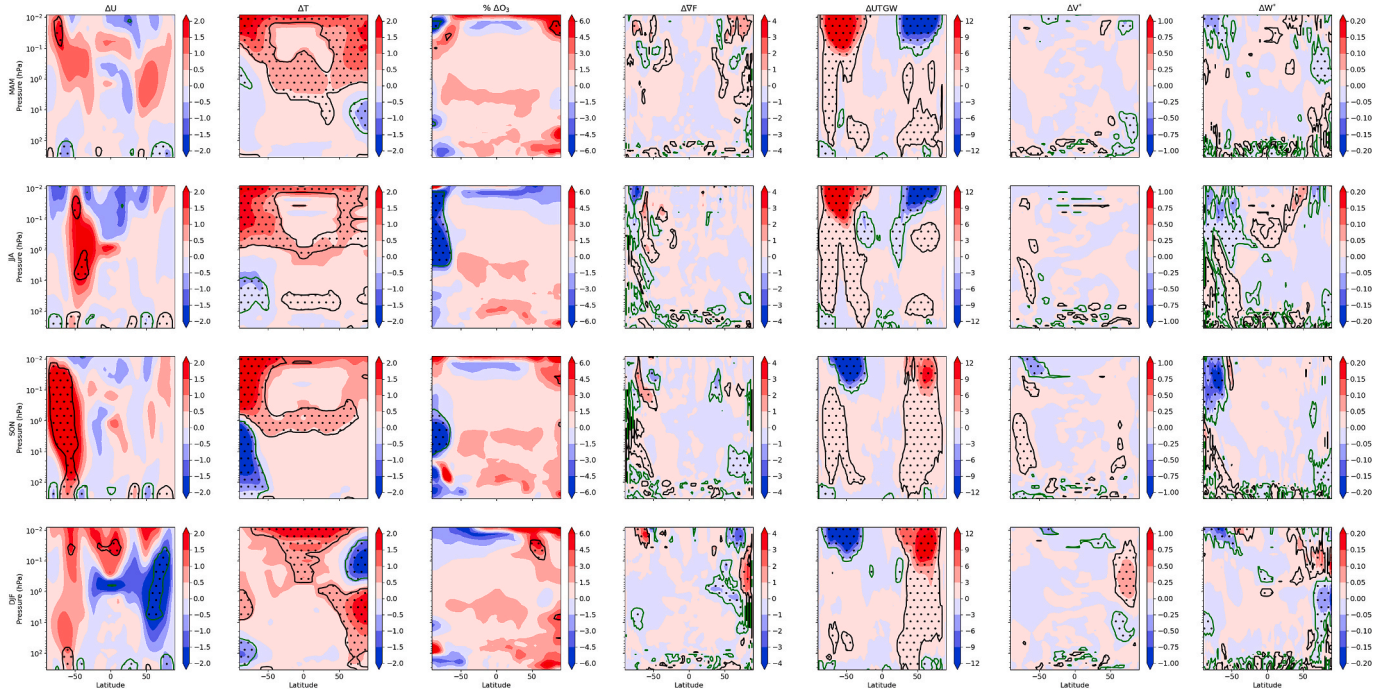

Fig. 13. As Fig. 12, but for differences H7-L3.

L7-L3

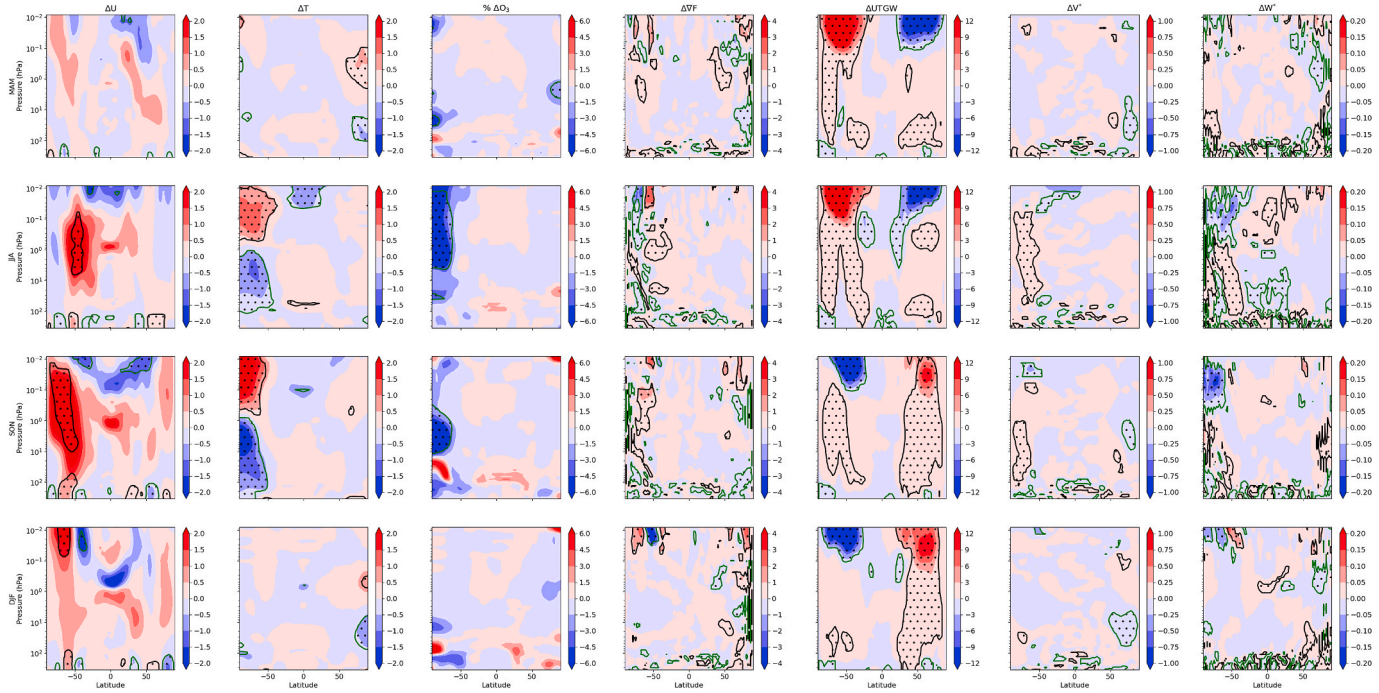

Fig. 14. As Fig. 12, but for differences L7-L3.

H7-H3

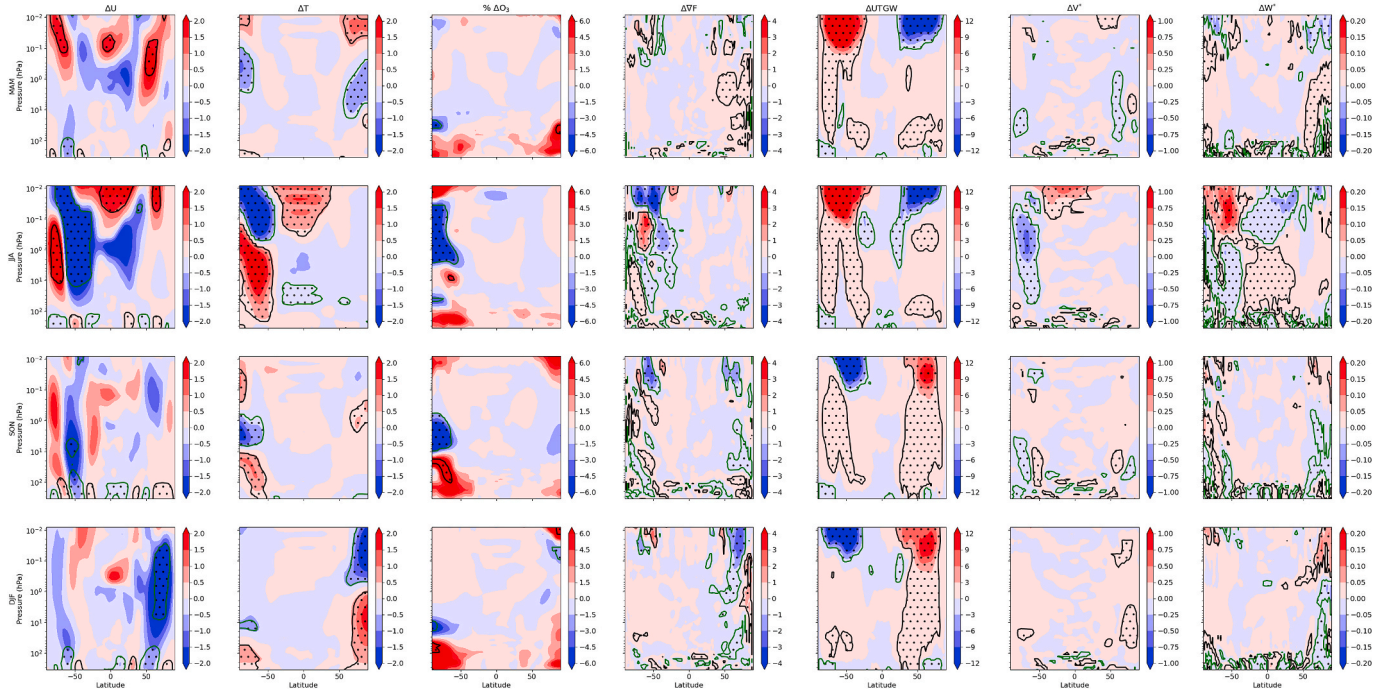

Fig. 15. As Fig. 12, but for differences H7-H3.

Declaration of competing interest

The authors declare that they have no known competing financial interests or personal relationships that could have appeared to influence the work reported in this paper.

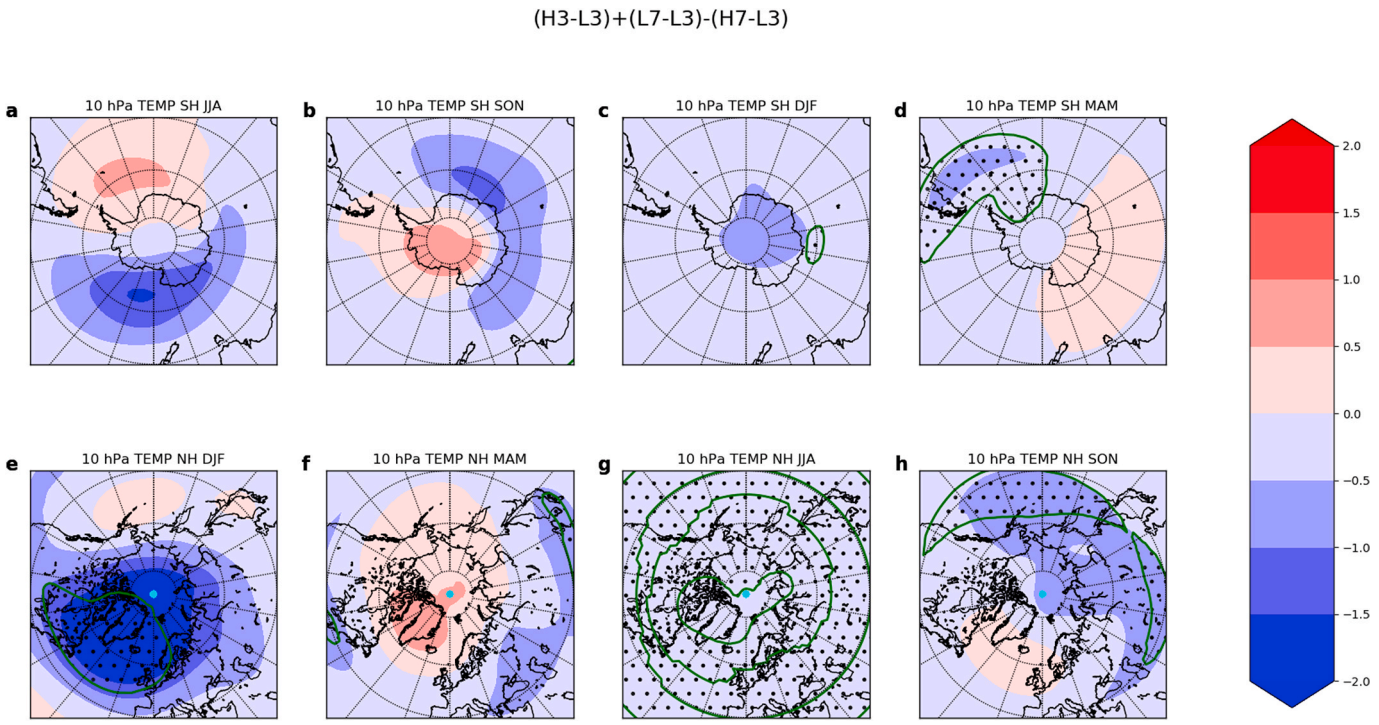

Fig. 16. 10 hPa temperature difference (K) between (H3-L3)+(L7-L3) and (H7-L3) values. The green line delimiting negative dotted areas indicates that the differences are statistically significant at 5% with a permutation test.

Acknowledgement

This work is funded by the project SOLENA – Solar effects on natural climate variability in the North Atlantic and Arctic – The Research Council of Norway, Program for Space Research Project: 255276/E10. The simulations were performed on resources provided by UNINETT Sigma2 – the National Infrastructure for High Performance Computing and Data Storage in Norway (NN9206K, NS9206K, NN9133K, NS9133K).

We are extremely grateful to two reviewers for their valuable comments, corrections and suggestions.

References

Baumgaertner, A.J.G., Jöckel, P., Brühl, C., 2009. Energetic particle precipitation in ECHAM5/MESSy1 – Part 1: downward transport of upper atmospheric NOx produced by low energy electrons. Atmos. Chem. Phys. 9, 2729–2740. https://doi.org/10.5194/acp-9-2729-2009.

Baumgaertner, A.J.G., Seppälä, A., Jöckel, P., Clilverd, M.A., 2011. Geomagnetic activity related NOx enhancements and polar surface air temperature variability in a chemistry climate model: modulation of the NAM index. Atmos. Chem. Phys. 11, 4521–4531. https://doi.org/10.5194/acp-11-4521-2011.

Brasseur, G., Solomon, S., 2005. Aeronomy of the Middle Atmosphere: Chemistry and Physics of the Stratosphere and Mesosphere, third ed. Springer, Dordrecht, the Netherlands, p. 646.

Callis, L., Natarajan, M., Lambeth, J.D., 2001. Solar-atmospheric coupling by electrons (SOLACE): 3. Comparisons of simulations and observations, 1979 – 1997, issues and implications. J. Geophys. Res. 106, 7523–7539. https://doi.org/10.1029/2000JD900615.

Callis, L., Boughner, R., Baker, D., Mewaldt, R., Bernard Blake, J., Selesnick, R., Cummings, J., Natarajan, M., Mason, G., Mazur, J., 1996. Precipitating electrons: evidence for effects on mesospheric odd nitrogen. Geophys. Res. Lett. 23, 1901–1904. https://doi.org/10.1029/96GL01787.

Chen, P., Holton, J.R., O'Neill, A., Swinbank, R., 1994. Quasi-horizontal transport and mixing in the Antarctic stratosphere. J. Geophys. Res. 99, 16851–16866. https://doi.org/10.1029/94JD00784.

Cullens, C.Y., England, S.L., Garcia, R.R., 2016. The 11 year solar cycle signature on wave-driven dynamics in WACCM. J. Geophys. Res.: Space Phys. 121, 3484–3496. https://doi.org/10.1002/2016JA022455.

Du, Z.L., 2011. The correlation between solar and geomagnetic activity – Part 2: long-term trends. Ann. Geophys. 29, 1341–1348. https://doi.org/10.5194/angeo-29-1341-2011 doi:10.5194/angeo-29-1341-2011.

Echer, E., Gonzalez, W.D., Gonzalez, A.L.C., Echer, E., Gonzalez, W.D., Gonzalez, A.L.C., Prestes, A., Vieira, L.E.A., dal Lago, A., Guarnieri, F.L., Schuch, N.J., 2004. Long-term correlation between solar and geomagnetic activity. J. Atmos. Sol. Terr. Phys. 66, 1019–1025. https://doi.org/10.1016/j.jastp.2004.03.011.

Edmon Jr., H., Hoskins, B., McIntyre, M., 1980. Eliassen-Palm cross sections for the troposphere. J. Atmos. Sci. 37, 2600–2616. https://doi.org/10.1175/1520-0469(1980)037<2600:EPCSFT>2.0.CO;2.

Fraser-Smith, A.C., 1972. Spectrum of the geomagnetic activity index Ap. J. Geophys. Res. 77, 4209–4220. https://doi.org/10.1002/grl.50711.

Funke, B., López-Puertas, M., Gil-López, S., von Clarmann, T., Stiller, G.P., Fischer, H., Kellmann, S., 2005. Downward transport of upper atmospheric NOx into the polar stratosphere and lower mesosphere during the Antarctic 2003 and Arctic 2002/2003 winters. J. Geophys. Res. 110, D24308. https://doi.org/10.1029/2005JD006463.

Garcia, R.R., 1992. Transport of thermospheric NOX to the stratosphere and mesosphere. Adv. Space Res. 12 (10), 57–66. https://doi.org/10.1016/0273-1177(92)90444-3.

Heath, D.F., Krueger, A.J., Crutzen, P.J., 1977. Solar proton event: influence on stratospheric ozone. Science 197, 886–889. https://doi.org/10.1126/science.197.4306.886.

Homeyer, C.R., Bowman, K.P., 2013. Rossby wave breaking and transport between the tropics and extratropics above the subtropical jet. J. Atmos. Sci. 70, 607–626. https://doi.org/10.1175/JAS-D-12-0198.1.

T. L. Homeyer, C.R., Bowman, K.P., Pan, L.L., Atlas, E.L., Gao, R.-S., Campos, T.L., 2011. Dynamical and chemical characteristics of tropospheric intrusions observed during START08 J. Geophys. Res. 116, D06111. https://doi.org/10.1029/2010JD015098.

Isaksen, I., Zerefos, C., Wang, W.-C., Balis, D., Eleftheratos, K., Rognerud, B., Stordal, F., Berntsen, T.K., LaCasce, J.H., Søvde, O.A., Olivié, D., Orsolini, Y.J., Zyrichidou, I., Prather, M., Tuinder, O.N.E., 2012. Attribution of the Arctic ozone column deficit in March 2011. Geophys. Res. Lett. 39 https://doi.org/10.1029/2012GL053876.

Jackman, C.H., McPeters, R.D., 2004. The effect of solar proton events on ozone and other constituents. In: Pap, J.M., Fox, P. (Eds.), Solar Variability and its Effects on Climate. Geophys. Monogr. Ser., vol. 141. AGU, Washington, D. C, pp. 305–319.

Katz, R.W., Brown, B.G., 1991. The problem of multiplicity in research on teleconnections'. Int. J. Climatol. 11, 505–513. https://doi.org/10.1002/joc.3370110504.

Kinnison, D.E., Brasseur, G.P., Walters, S., Garcia, R.R., Marsh, D.R., Sassi, F., Harvey, V. L., Randall, C.E., Emmons, L., Lamarque, J.F., Hess, P., Orlando, J.J., Tie, X.X., Randel, W., Pan, L.L., Gettelman, A., Granier, C., Diehl, T., Niemeier, U., Simmons, A.J., 2007. Sensitivity of chemical tracers to meteorological parameters in the MOZART-3 chemical transport model. J. Geophys. Res. 112, D20302. https://doi.org/10.1029/2006JD007879.

Kodera, K., Kuroda, Y., 2002. Dynamical response to the solar cycle. J. Geophys. Res. 107 (D24), 4749. https://doi.org/10.1029/2002JD002224.

Kuchar, A., Sacha, P., Miksovsky, J., Pisoft, P., 2015. The 11-year solar cycle in current reanalyses: a (non)linear attribution study of the middle atmosphere. Atmos. Chem. Phys. 15, 6879–6895. https://doi.org/10.5194/acp-15-6879-2015.

Kvissel, O.-K., Orsolini, Y.J., Stordal, F., Isaksen, I.S.A., Santee, M.L., 2012. Formation of stratospheric nitric acid by a hydrated ion cluster reaction: implications for the effect

of energetic particle precipitation on the middle atmosphere. J. Geophys. Res. 117, D16301. https://doi.org/10.1029/2011JD017257.
Langematz, U., Kunze, M., Krueger, K., Labitzke, K., Roff, G.L., 2003. Thermal and dynamical changes of the stratosphere since 1979 and their link to ozone and CO2 changes. J. Geophys. Res. 108 (D1), 4027. https://doi.org/10.1029/2002JD002069.
Langford, A.O., Proffitt, M.H., Vanzandt, T.E., 1996. Modulation of tropospheric ozone by a propagating gravity wave. J. Geophys. Res. Atmos. 101, 26605–26613. https://doi.org/10.1029/96JD02424.
Larkin, A., Haigh, J.D., Djavidnia, S., 2000. The effect of solar UV irradiance variations on the earth's atmosphere. Space Sci. Rev. 94, 199–214. https://doi.org/10.1023/A:1026771307057.
Lin, S., Rood, R.B., 1997. An explicit flux-form semi-Lagrangian shallow-water model on the sphere. Q. J. R. Meteorol. Soc. 123, 2477–2498. https://doi.org/10.1002/qj.49712354416.
Lu, H., Jarvis, M.J., Graf, H.-F., Young, P.C., Horne, R.B., 2007. Atmospheric temperature responses to solar irradiance and geomagnetic activity. J. Geophys. Res. 112, D11109. https://doi.org/10.1029/2006JD007864.
Lu, H., Jarvis, M.J., Hibbins, R.E., 2008. Possible solar wind effect on the northern annular mode and northern hemispheric circulation during winter and spring. J. Geophys. Res. 113, D23104. https://doi.org/10.1029/2008JD010848.
Maliniemi, V., Asikainen, T., Mursula, K., 2014. Spatial distribution of Northern Hemisphere winter temperatures during different phases of the solar cycle. J. Geophys. Res.: Atmosphere 119, 9752–9764. https://doi.org/10.1002/2013JD021343.
Marsh, D.R., Garcia, R.R., Kinnison, D.E., Bouville, B.A., Sassi, F., Solomon, S.C., Matthes, K., 2007. Modeling the whole atmosphere response to solar cycle changes in radiative and geomagnetic forcing. J. Geophys. Res. 112, D23306 https://doi.org/10.1029/2006JD008306.
Marsh, D.R., Mills, M., D Kinnison, D., Lamarque, J.-F., Calvo, N., L Polvani, L., 2013. Climate change from 1850 to 2005 simulated in CESM1(WACCM). J. Clim. 26, 7372–7391. https://doi.org/10.1175/JCLI-D-12-00558.
Meraner, K., Schmidt, H., 2018. Climate impact of idealized winter polar mesospheric and stratospheric ozone losses as caused by energetic particle precipitation. Atmos. Chem. Phys. 18, 1079–1089. https://doi.org/10.5194/acp-18-1079-2018.
Müller, R., Tilmes, S., Konopka, P., Grooß, J.-U., Jost, H.-J., 2005. Impact of mixing and chemical change on ozone-tracer relations in the polar vortex. Atmos. Chem. Phys. 5, 3139–3151. https://doi.org/10.5194/acp-5-3139-2005.
Myllys, M., Kilpua, E., Pulkkinen, T., 2015. Solar-wind control of plasma sheet dynamics. Ann. Geophys. 33, 845–855. https://doi.org/10.5194/angeo-33-845-2015.
Neale, R.B., Coauthors, 2012. Description of the NCAR Community Atmosphere Model (CAM5.0), NCAR Tech. Note, NCAR/TN-4861STR. Natl. Cent. For Atmos. Res, p. 274. Available at: http://www.cesm.ucar.edu/models/cesm1.0/cam/docs/description/cam5_desc.pdf. (Accessed 7 February 2020).
Nikulin, G., Karpechko, A., 2005. The mean meridional circulation and midlatitude ozone buildup. Atmos. Chem. Phys. 5, 3159–3172. https://doi.org/10.5194/acp-5-3159-2005.
Orsolini, Y.J., Limpasuvan, V., Perot, K., Espy, P.J., Hibbins, R.E., Lossow, S., Larsson, K. R., Murtagh, D., 2017. Modelling the descent of nitric oxide during the elevated stratopause event of January 2013. J. Atmos. Sol. Terr. Phys. 155, 50–61. https://doi.org/10.1016/j.jastp.2017.01.006.
Orsolini, Y.J., Manney, G.L., Santee, M.L., Randall, C.E., 2005. An upper stratospheric layer of enhanced HNO_3 following exceptional solar storms. Geophys. Res. Lett. 32, L12S01 https://doi.org/10.1029/2004GL021588.
Peck, E.D., Randall, C.E., Harvey, V.L., Marsh, D.R., 2015. Simulated solar cycle effects on the middle atmosphere: WACCM3 versus WACCM4. J. Adv. Model. Earth Syst. 7, 806–822. https://doi.org/10.1002/2014MS000387.
Randall, C.E., Harvey, V.L., Manney, G.L., Orsolini, Y., Codrescu, M., Sioris, C., Brohede, S., Haley, C.S., Gordley, L.L., Zawodny, J.M., Russell III, J.M., 2005. Stratospheric effects of energetic particle precipitation in 2003–2004. Geophys. Res. Lett. 32, L05802. https://doi.org/10.1029/2004GL022003.
Randall, C.E., Rusch, D.W., Bevilacqua, R.cM., Hoppel, K.W., Lumpe, J.D., 1998. Polar ozone and aerosol measurement (POAM) II stratospheric NO 2. J. Geophys. Res. 103 (D21), 28,361–28,371. https://doi.org/10.1029/98JD02092.
Randall, C.E., Siskind, D.E., Bevilacqua, R.M., 2001. Stratospheric NOx enhancements in the southern hemisphere vortex in winter/spring of 2000. Geophys. Res. Lett. 28 (12), 2385–2388. https://doi.org/10.1029/2000GL012746.
Roble, R., Ridley, E., 1987. An auroral model for the NCAR thermospheric general circulation model (tgcm). Ann. Geophys. - Ser. A Up. Atmos. Space Sci. 5, 369–382.
Sabutis, J.L., 1997. The short-term transport of zonal mean ozone using a residual mean circulation calculated from observations. J. Atmos. Sci. 54, 1094–1106. https://doi.org/10.1175/1520-0469(1997)054<1094:TSTTOZ>2.0.CO;2.
Schoeberl, M.R., Hartmann, D.L., 1991. The dynamics of the stratospheric polar vortex and its relation to springtime ozone. Science 251, 46–52.
Seppälä, A., Lu, H., Clilverd, M.A., Rodger, C.J., 2013. Geomagnetic activity signatures in wintertime stratosphere wind, temperature, and wave response. J. Geophys. Res. Atmos. 118, 2169–2183. https://doi.org/10.1002/jgrd.50236.
Seppälä, A., Verronen, P.T., Clilverd, M.A., Randall, C.E., Tamminen, J., Sofieva, V., Backman, L., Kyrölä, E., 2007. Arctic and Antarctic polar winter NOx and energetic particle precipitation in 2002-2006. Geophys. Res. Lett. 34, L12810. https://doi.org/10.1029/2007GL029733.
Smith-Johnsen, C., Marsh, D.R., Orsolini, Y., Nesse Tyssøy, H., Hendrickx, K., Sandanger, M.I., et al., 2018. Nitric oxide response to the April 2010 electron precipitation event: using WACCM and WACCM-D with and without medium-energy electrons. J. Geophys. Res.: Space Phys. 123, 5232–5245. https://doi.org/10.1029/2018JA025418.
Solomon, S., Barth, C.A., Bailey, S.M., 1999. Auroral production of nitric oxide measured by the SNOE satellite. Geophys. Res. Lett. 26 (9), 1259–1262. https://doi.org/10.1029/1999GL900235.
Solomon, S., Crutzen, P.J., Roble, R.G., 1982. Photochemical coupling between the thermosphere and the lower atmosphere 1. Odd nitrogen from 50 to 120 km. J. Geophys. Res. 87 (C9), 7206–7220. https://doi.org/10.1029/JC087iC09p07206.
Storch, H.v., 1982. A remark on Chervin-Schneider's algorithm to text significance. J. Atmos. Sci. 39, 187–189. https://doi.org/10.1175/1520-0469(1982)039<0187:AROCSA>2.0.CO;2.
Tapping, K.F., 2013. The 10.7 cm solar radio flux (F10.7). Space Weather 11, 394–406. https://doi.org/10.1002/swe.20064.
Tartaglione, N., Toniazzo, T., Orsolini, Y., Otterå, O.H., 2020. A note on the statistical evidence for an influence of geomagnetic activity on Northern Hemisphere seasonal-mean stratospheric temperatures using the Japanese 55-year Reanalysis. Ann. Geophys. 38, 545–555. https://doi.org/10.5194/angeo-38-545-2020.
Tomikawa, Y., 2017. Response of the middle atmosphere in the southern hemisphere to energetic particle precipitation in the latest reanalysis data. SOLA 13A, 1–7. https://doi.org/10.2151/sola.13A-001.
Turunen, E., Kero, A., Verronen, P.T., Miyoshi, Y., Oyama, S., Saito, S., 2016. Mesospheric ozone destruction by high-energy electron precipitation associated with pulsating aurora. J. Geophys. Res.: Atmosphere 121, 11852–11861. https://doi.org/10.1002/2016JD025015.
Wigley, T.M.L., Santer, B.D., 1990. Statistical comparison of spatial fields in model validation, perturbation, and predictability experiments. J. Geophys. Res. 95 (D1), 851–865. https://doi.org/10.1029/JD095iD01p00851.
Wilks, D.S., 2006. Statistical Methods in the Atmospheric Sciences. Elsevier Science, Burlington, MA.
Wilks, D.S., 2016. The stippling shows statistically significant grid-points. How research results are routinely overstated and over interpreted, and what to do about it. Bull. Am. Meteorol. Soc. 97, 2263–227,. https://doi/10.1175/bams-d-15-00267.1.